Crop Water Productivity Estimation for Resilient Agriculture Using Remote Sensing and Machine Learning Approach

by

Alfred Amboka

Project research report submitted to the department of Geomatic Engineering and Geospatial Information Systems for the award of degree of Bachelor of Science in Geomatic Engineering and Geospatial Information Systems (GEGIS), 2023.

Department of Geomatic Engineering and Geospatial Information Systems (GEGIS)

DECLARATION

I declare that this project is my own work and has not been submitted by anybody else in any other university for the award of any degree to the best of my knowledge.

Sign…… Date……...

Alfred Amboka

ENC221-0099/2018

Department of Geomatic Engineering and Geospatial Information Systems (GEGIS)

Jomo Kenyatta University of Agriculture and Technology

CERTIFICATION

This project has been submitted for examination with my approval as the candidate's supervisor.

Sign……. Date ……

Mr. Moffat Magondu

Senior Lecturer, GEGIS

Department of Geomatic Engineering and Geospatial Information Systems (GEGIS)

Acknowledgements

#####

Abstract

##########

Table of contents

List of figures

List of tables

Acronyms and abbreviations

1 Introduction

1.1 Background

Agriculture is the backbone of many economies, providing food and livelihoods for millions of people worldwide. However, the increasing demand for food coupled with the effects of climate change has put a strain on water resources leading to water scarcity in many regions. Water scarcity refers to the limited availability of freshwater resources to meet the demands of various sectors, including agriculture. This is a significant challenge that affects agricultural production and food security in many regions of the world (Booker & Trees, 2020). Agriculture fully depends on water which can be both rainfed or irrigated. Estimation of water used and yield produced is therefore necessary. This is enhanced through crop water productivity.

Crop water productivity (CWP) is generally defined as crop yield per cubic meter of water consumption or the ratio of yields to evapotranspiration during the growing season

(H. Gao et al., 2023; Hellegers et al., 2009). Crop water productivity estimation is a crucial aspect of precision agriculture, which aims to optimize the use of agronomic inputs like water, pesticides, and fertilizers to meet the growing demand for food while minimizing the use of natural resources like land and fresh water. The productivity of crops can vary depending on whether they are grown in rain-fed or irrigated agriculture systems.

Irrigated agriculture accounts for an estimated 70% of total freshwater withdrawals worldwide, and in many drier countries, agricultural water use accounts for more than 90% of total withdrawals (Scheierling & Tréguer, 2018). As water becomes increasingly scarce, the management of agricultural irrigation moves to the center of water management concerns. Without advances in management and more integrated policy-making in developed and developing countries, water scarcity, and related water problems will significantly worsen over the next several decades. The transition from an expansionary water economy to a maturing water economy has led to the need for more efficient water use in agriculture. The concept of water productivity, which denotes the relationship between marketable yield and the seasonal water use by the plant through evapotranspiration, is an important indicator to express the resource use efficiency and can provide an assessment of crop performance under different irrigation strategies (Hommadi &

Almasraf, 2019). Rain-fed agriculture, on the other hand, is characterized by low average yields compared to irrigated agriculture, as rainfall rarely meets the time with the required amount of water application for plant growth. The performance of rain-fed productivity remains low and stable for most crops, and crop production is undulating under rain-fed agriculture. In many countries, rain-fed areas are the critical cultivation areas with the largest concentration of rural poverty spanning several agroecological regions. The low efficiency of water use efficiency and management in agriculture is a major challenge and one of the contributing factors to low crop productivity and balance is drought.

Estimations of CWP are affected by drought conditions. Therefore, understanding the climatic conditions of the region of interest is paramount while carrying out such studies. According to (Sarshad et al., 2021), drought is the greatest environmental stress in arid and semiarid regions which has restricted agricultural development. Those agricultural activities that have to survive in such areas are exposed to extreme temperatures, variations in rainfall, long solar radiation hours, and so on. Kenya is particularly vulnerable to drought due to its geography and climate. Several droughts are common in agricultural lands in Kenya and most tropical regions. The different types of droughts, their severity, and their impacts depend on various factors, such as the duration, intensity, and spatial extent of the drought event. Meteorological drought is the most common type of drought, which occurs when there is a prolonged period of below-average precipitation. Agricultural drought refers to the impact of meteorological drought on crop production, while hydrological drought is characterized by low water availability in rivers, lakes, and groundwater. As drought impact on agriculture influences crop evapotranspiration (ET) and general yield obtained hence the need to look into how to manage available water resources for maximum production in drought conditions. This brings us to why CWP has established itself as a recognized indicator for evaluating the progress being made toward SDG 6.4, which calls for much greater water usage efficiency (Blatchford et al., 2018; Ghorbanpour et al., 2022).

The level of CWP estimation varies with scale, including at the farm level, and regional level. The robustness of such estimation is influenced by several factors including data and the extent of the study area. Farm-level estimation is challenging and is limited in one way considering the high volume of estimation data required when performing time series estimation. Traditionally, estimating CWP has relied on labor-intensive and time-consuming field-based methods, such as

lysimeters and soil moisture sensors. These methods are often limited in spatial coverage and cannot provide real-time data for large-scale agricultural areas. Moreover, they may not account for spatial variations in soil moisture and crop water requirements within a field. This has given way to the use of remote sensing for crop water productivity estimations. Remote sensing can help estimate actual evapotranspiration (ET) and crop yield, which are important factors in CWP estimation (Ghorbanpour et al., 2022; Gao et al., 2023). This is important for improving regional agricultural water use efficiency and water conservation levels. Finally, remote sensing coupled with machine learning has been on the rise in many fields including agriculture and water use efficiency estimation.

Machine learning is becoming an increasingly popular tool for estimating crop water productivity. Existing methods of machine learning continue to prove to be more reliable through data fusion and the combination of several models (Elbeltagi et al., 2022). On remote sensing data for farming, many machine learning algorithms have been applied, including random forests (RFs), support vector machines (SVMs), artificial neural networks (ANNs), genetic algorithms (GAs), and ensemble learning (Virnodkar et al., 2020; Sadri et al., 2022). Particularly in geographic classification and remote sensing data prediction, RF applications have gained popularity for resolving data overfitting (Sadri et al., 2022; Vergopolan et al., 2021; (Saini & Ghosh, 2018). Although machine learning has been used in many fields such as yield estimation (Islam et al., 2023), and weather forecasting (Patel et al., 2021) together with remote sensing, it is underutilized in crop water productivity estimation. The variation is from the global level to the country and local level. Therefore, this study focuses on CWP estimation at the local level and specifically in irrigation schemes in the eastern part of Kenya - Bura Tana River Scheme.

The Bura Irrigation Scheme covers a total area of 5,360 hectares, although only 3,340 hectares are now used for irrigation due to a lack of water resources. Still, there is potential to enhance water availability, allowing irrigation of greater areas and increasing maize output, which is now at a low level. The plan now yields 3.5 tons per hectare of commercial maize and 4.4 tons per hectare of seed maize.(Muigai David et al., 2019). This is less than the 4.9 t ha-1 average for the entire world value. Accurate water management in this area is therefore essential and proper estimates of how water is used and yield produced will be of importance. The use of machine learning coupled with remote sensing will allow proper mitigation measures to be applied.

Therefore, CWP estimation is necessary to boost production while withstanding drought conditions and help reduce the growing water scarcity levels.

1.2 Statement of the Problem

One of the significant challenges in agricultural systems particularly in irrigation schemes in Kenya is the limited availability of water resources. Water scarcity continues to increase due to the impact of climate change. According to the UN, 2022 report, over 85% of the wetlands on our planet have been lost for over 300 years. The problem of the water crisis has been made worse by factors such as water contamination, population increase, urbanization, and inadequate management of water resources. Therefore, food security is going to be impacted by water shortage (Mulwa et al., 2021). On the other hand, drought continues to rage in Kenya, resulting in reduced agricultural land and affecting agricultural production, especially in the supply of water for production.

The physiological and biochemical processes of plants are predicted to be affected by soil water stress, which is a major barrier to agricultural production, particularly in arid and semi-arid lands (ASALs) (M. N. et al., 2015); Mbayaki, 2021). By managing crops and water poorly, plant quality and yields may be harmed (Fan et al., 2012; Mbayaki, 2021).

Accurate estimation of CWP requires comprehensive data on crop growth, soil moisture, and water availability. However, obtaining such data is challenging and often needs to be improved in the Bura Irrigation Scheme. Existing methods of water productivity being used are limited and the data being used is a major contribution to this effect. Bura Irrigation scheme being among the largest in Kenya has faced low records of yield production as outlined in a paper done by (Muigai et al., 2019). The scheme relies on water from river Tana which is 50 km away. Over the recent years, the river Tana water level has been reducing due to drought effects upstream. This impact the supply of water for agricultural purpose downstream including the Bura Irrigation scheme. In such scenarios, it becomes crucial to optimize water use efficiency to ensure sustainable and resilient agriculture. However, conventional irrigation practices often result in inefficient water use and lower crop water productivity. There is a need to address this problem by developing methods to estimate and improve crop water productivity by utilizing remote sensing (RS) and machine learning techniques. By accurately assessing water requirements and usage patterns,

effective water management strategies can be devised to enhance agricultural productivity while conserving water resources.

1.3 Justification

Water scarcity continues to rage in arid and semi-arid lands due to drought. Bura Irrigation scheme which is within agro-ecological zone V (semi-arid to arid) obtains its water from the Tana River which is 50 km away by pumping water from the river (National Irrigation Authority, 2023) In addition, the area experiences low rainfall of about 400mm. High Temperatures are experienced all year round with little seasonal variation. Mean maximum temperatures never fall below 31°C and average minimum temperatures are above 20°C. All these factors make the agricultural area more vulnerable and costly, especially in the case of water pumping to meet crop water needs in the area. Water Crop water productivity is a crucial requirement for increased agricultural production because crop water is needed to substitute for water loss by transpiration and soil evaporation (Mbayaki, 2021)

Over the recent years, food insecurity has affected many parts of Kenya with Eastern and Northern regions being highly affected. According to the Integrated Food Security Phase Classification (IPC), 2023, an estimated of around 4.4 million people in ASALs are facing acute food insecurity. Generally, in Kenya, acute food insecurity has affected around 37% of the population between 2022 and 2023 and is expected to increase. Food insecurity continues to rise with increasing agricultural drought events, rapid population growth, water pollution reducing water use for agricultural purposes, and high demand that strains available water resources. In addition, Kenya declared In September 2021, the East African state of Kenya drought emergency. The affected drought areas (ASALs) continually received low rainfall for the season between November and December (International Committee of the Red Cross, 2022) leading to low agricultural production. With all these cases of drought events, agricultural production can be optimized to survive in the face of water scarcity to boost productivity by managing available water resources. CWP serves as the best alternative for the estimation of crop productivity in existing irrigation schemes and may serve as a near real-time decision-making tool on water management to increase agricultural production hence an increase in food security.

1.4 Research identification and Objectives

The main objective is to estimate crop water productivity using remote sensing and machine learning techniques for a period between 2018 to 2022 in Bura irrigation scheme which can help support irrigation management and improve agricultural resilience. Specific objectives include:

- To estimate maize yield and determine evapotranspiration (ET) values based on analyzed maize crop phenological period in the study area,
- To estimate maize crop water productivity and analyze the spatial distribution of CWP,
- To develop machine learning models for the estimation of crop water productivity (CWP) for maize crops and identify the best-performing machine learning models for CWP estimation in the study area.

1.5 Study outline

This research study is divided into 6 chapters whereby the first chapter introduces

the study by detailing the background, statement of the problem, justifying the problem, and objectives; Chapter 2 contains the reviewed literature that relates to this topic. Further, Chapter 3 shows the data and methods used in the study with Chapter 4 highlighting the results for the findings from the methods. Chapter 5 discusses the findings and finally, Chapter 6 concludes and recommends future research that might not be addressed at this level of geoscientific exploration and expertise.

2. Literature review

2.1 Water Use, and Water Productivity

Crop water productivity (CWP) is an important concept in agronomy that seeks to maximize viable yields per unit of water used in both rain-fed and irrigated agricultural operations. CWP may be accomplished by increasing crop marketable yields per unit of transpired water and decreasing water loss from the soil water balance (Mbayaki, 2021). Water use and water use efficiency all refer to CWP and are frequently used synonymously.

Crop water productivity (CWP) plays an essential role in irrigated agriculture for food and security of the environment, especially when water becomes limited. (Bekchanov et al., 2012). Estimates have already been made using crop models in previous research. Crop modeling is an effective method for calculating WP and plays an important part in water management methods. (Soomro et al., 2019). Commonly used crop models for maize include CERES-Maize (Crop Environment Resource Synthesis), SWAT, SWAP (Soil Water Atmosphere Plant), AQUACROP, CROPWAT, and more. The CERES-Maize model (Cuculeanu et al., 2002), is specifically designed to simulate the growth, development, and yield of maize (corn) crops under different agroclimatic and management conditions. It has been widely used to assess crop water productivity for maize and to study the impact of water management strategies on maize production (Kisekka et al., 2017; Sen et al., 2023). The model incorporates a comprehensive water balance approach, which takes into account various water inputs and outputs for the maize crop. These inputs include rainfall, irrigation, and soil water content, while outputs include evapotranspiration (ET) and drainage losses. The model estimates how efficiently the maize crop uses water to produce yield by simulating the water balance. Nonetheless, other crop models can accurately estimate crop water productivity, such as the FAO Aqua Crop model. The Aqua Crop model simulates attainable yields of major herbaceous crops as a function of water consumption under rainfed, supplemental, deficit, and full irrigation conditions. Similarly, the model has been widely used to assess water productivity (Mostafa et al., 2023; (Shan et al., 2023). Additionally, some studies have proposed a combined method for the estimation of spatial and temporal variation of crop water productivity under deficit irrigation scenarios based on the Aqua Crop model (Ahmadpour et al., 2022).

2.2 Crop Water Productivity Estimation

The CWP estimation is achieved by the ratio of yield and actual evapotranspiration (ETa) (Talpur et al., 2023; Yihun et al., 2013).

The phenological period, which refers to the different stages of crop growth and development, plays a crucial role in estimating ET and crop yield (H. Gao et al., 2023). Factors such as crop coefficient (Kc) and harvest index (HI), which vary during different phenological periods, are considered in the estimation of ET and yield. Different crops have varying crop phenology growing periods, quantity harvested, and crop response to the environmental conditions influence crop yield. Crop transpiration is calculated by multiplying the reference evapotranspiration (ETo) with a crop coefficient (KcTr). According to FAO, the crop coefficient is proportional to canopy cover and varies throughout the life cycle of a crop. It is affected by water stress, which can affect canopy development and induce stomata closure, thereby directly affecting crop transpiration. A study carried out by (H. Gao et al., 2023), utilized the dry matter mass–harvest index, crop Kc based on crop phenology to map crop water productivity of maize and wheat to be 1.60 kg/m3 and 1.39 kg/m3 respectively in the area of study.

The evapotranspiration (ET) formula is used to estimate the amount of water used by crops. The ET formula takes into account various factors such as temperature, humidity, wind speed, and solar radiation. The Penman-Monteith equation is a widely used ET formula that is recommended by the Food and Agriculture Organization (FAO) of the United Nations. The Penman-Monteith equation is a combination of energy balance and aerodynamic resistance equations and is considered the most accurate method for estimating ET. (Wang et al., 2023; (Hassan et al., 2022) and more employed the ET formula in the estimation of evapotranspiration which is an important component of CWP estimation.

To estimate the crop water productivity of maize, several studies have been conducted using different methods and models. A study carried out in Mexico used locally developed crop coefficient curves and United Nations Food and Agriculture Organization (FAO) crop coefficients to estimate maize water use and water productivity. The study found that maize actual evapotranspiration varied with year and ranged from 634.2 to 697.7 mm by the local Kc curve, from 687.3 to 739.3 mm by the non-adjusted FAO Kc values, and from 715.8 to 779.6 mm with the FAO adjusted Kc values. One study proposed an ensemble approach for identifying the virtual

water content (VWC) of main crops on the Korean Peninsula in past and future climates. The ensemble VWC is calculated using three types of crop yields and fifteen consumptive amounts of water use in the past and the future (Lim et al., 2017). The study found that while the ensemble VWC of rice and maize was 1.18 m3 kg−1 and 0.58 m3 kg−1, respectively, in the past, the future amounts were estimated at 0.76 m3 kg−1 and 0.48 m3 kg−1, respectively. The yields of both crops showed a decline in future projections, indicating that this change could have a positive impact on future water demand.

3.8 Machine Learning

3.8.1 Machine learning models used to estimate Yield, ETa, and CWP.

This section utilizes three machine learning models, namely: Random Forest Regressor, Support vector machine, and Extreme Gradient Boosting.

Random Forest (RF) is an ensemble method that leverages the power of multiple decision trees by training them on diverse subsets of the training data through bootstrapping, ultimately creating a robust and integrated learning algorithm (Elbeltagi et al., 2022). The outcome of Random Forest (RF) approximations consists of the averages from each individual tree. As a result, RF provides the capability to reduce variance and achieve more accurate predictions when compared to typical tree-based algorithms. Nonetheless, in cases of predicting extreme observations, it can introduce bias. Specifically, when dealing with a small number of observations, RF predictions tend to be overly optimistic, while for larger datasets, RF predictions tend to be overly conservative. In this study, bias correction followed RF bias correction flow applied by (Zhao et al., 2022). The scikit-learn package (Pedregosa et al., 2011) was utilized to independently train Random Forest regressors on each dataset.

Support Vector Regression (SVR) is a machine learning approach grounded in Vapnik-Chervonenkis (VC) theory and the principle of Structural Risk Minimization (SRM). SVM is the machine learning algorithm that comes closest to deep learning. A two-layer neural network is equivalent to nonlinear SVM. A multi-layer neural network may be simulated by adding extra kernel functions to nonlinear SVM (Mountrakis et al., 2011). SVR extends its applicability to nonlinear regression tasks through the utilization of kernel functions, which help transform input

data into a higher-dimensional feature space. SVR incorporates the concept of slack variables during training, allowing the model to accommodate and tolerate certain errors. This inclusion of slack variables enhances the model's capacity for generalization (Xu et al., 2023). In the estimation of ET, Yield and CWP, the non-linear radial basis function kernel function is used. This type of kernel function performs better than other kernels for SVM model. The optimal hypermeters are determined where C for the kernel function is determined through trial and error.

Extreme Gradient Boosting (XGBoost) is a distributed gradient boosting library that has been built to be very efficient, adaptable, and portable. It employs machine learning methods using the Gradient Boosting framework. It utilizes a second-order Taylor expansion of the target function and utilizes the second derivative to enhance the speed of model convergence during training. Furthermore, a regularization component is incorporated into the target function to manage the complexity of the tree, resulting in a more straightforward model and guarding against overfitting (Geng et al., 2021). XGBoost introduces a novel sparsity-aware algorithm for handling sparse data and a weighted quantile sketch for approximate tree learning. The sparsity-aware algorithm is designed to efficiently handle sparse data, which is common in many real-world applications. It optimizes the tree construction process by only considering non-zero values, reducing the computational cost and memory usage. The weighted quantile sketch is a technique introduced in Xgboost to handle weighted data. It allows Xgboost to find quantiles on weighted data, which is important for accurate tree learning. This technique is the first method to solve the problem of finding quantiles on weighted data. In this study, some of the parameters of importance used for XGBoost includes n_estimators, learning_rate, max_depth, subsample, and colsample_bytree. More information about XGBoost can be found from the documentation.

3.8.2 Performance Metrics and Evaluation

Calculated data for ETa, CWP, and Yield are hereby compared to the modelled data. This is achieved through model performance evaluation. The dataset is spit into 70% Training and 30% validation. To cub model overfitting, K-fold cross validation method is employed. To perform cross-validation (CV) in this study, the dataset was split into k subdivisions specifically using a 5-fold CV. In each of the 5 iterations, the model was trained, and during each iteration, a different fold was held out from the training set and used as the validation set. This approach ensures that each fold has a turn at being the validation set while the model is trained multiple times.

Model performance is assessed using mean absolute error (MAE) Equation (20), coefficient of determination (R^2) Equation (21), mean square error (MSE) Equation (22), and root mean square error (RMSE) Equation (23) (Elbeltagi et al., 2022).

$$MAE = \frac{1}{n}\sum_{i=1}^{n}|y_i - \hat{y}_i| \tag{20}$$

$$R^2 = 1 - \frac{\sum_{i=1}^{n}(y_i - \hat{y}_i)^2}{\sum_{i=1}^{n}(y_i - \bar{y})^2} \tag{21}$$

$$MSE = \frac{1}{n}\sum_{i=1}^{n}(y_i - \hat{y}_i)^2 \tag{22}$$

$$RMSE = \sqrt{\frac{1}{n}\sum_{i=1}^{n}(y_i - \hat{y}_i)^2} \tag{23}$$

Where n is the sum of all points used, y_i is the observed calculated value of the respective values of ETa, CWP, or Yield that are the target or response variables. $\hat{y}$ represent the modelled values and ȳ represents the mean value of respective reference value of the target variables.

CWP Estimation Methods

Estimation methods vary depending on the region and the crops being cultivated. They are mainly grouped into field-based, modeling and simulation, and remote sensing and machine learning methods. Every method has its advantages and disadvantages.

2.2.1 Surface Energy Balance Algorithm (SEBAL)

SEBAL has proven to be a valuable tool for water resource management, agricultural planning, and environmental monitoring, providing reliable estimates of evapotranspiration and surface energy fluxes over large areas. It has been widely adopted in various research and operational applications worldwide due to its ability to utilize freely available satellite data and provide valuable information for water-scarce regions. The Surface Energy Balance Algorithm (SEBAL) is a method used to estimate evapotranspiration (ET) using remote sensing and the energy balance principle (Gibson et al., 2013). It was developed to analyze thermal infrared remote sensing data from satellites, such as the Landsat series, to monitor and manage water resources and agriculture efficiently. Souza et al., 2023 carried out a study that focused on estimating the evapotranspiration of irrigated açaí plants in eastern Amazonia using SEBAL. The results showed good agreement with the Bowen ratio method, and SEBAL was found to be useful for irrigation management and reducing water losses. Similarly, (Gao et al., 2023; Kamyab et al., 2022; Bansouleh et al., 2015; PACHAC HUERTA & CHÁVARRI VELARDE, 2019) and more recently used this model in the estimation of evapotranspiration proved to be more efficient. SEBAL is limited for accurate evapotranspiration Estimation. SEBAL relies on spatial information, such as land surface temperature and vegetation indices, which can vary across different areas. This spatial dependence can introduce uncertainties in the estimation of evapotranspiration. This is due to the reliance on anchor pixels. (Prakash Mohan et al., 2020), properly outline the limitation of anchor pixels. Another limitation of this Algorithm is wind speed observation SEBAL requires accurate wind speed data for calculating the dry/wet endpoints of each pixel. However, wind speed observations are known to have high temporal and spatial variations and may not be routinely available, especially in heterogeneous areas. SEBAL is sensitive to vegetation parameters, such as the Normalized Difference Vegetation Index (NDVI), which is used to estimate the fraction of vegetation cover. Inaccurate or incomplete vegetation information can affect the accuracy of SEBAL estimates (Ruhoff et al., 2012).

Surface Energy Balance System (SEBS) is another remote sensing-based algorithm used to estimate evapotranspiration (ET) and surface energy fluxes from satellite data. It was developed to overcome some limitations of the Surface Energy Balance Algorithm (SEBAL) and provide more accurate and physically based estimates of surface energy fluxes and ET. Similar to SEBAL,

there are discrepancies in the reported accuracy of the SEBS model due to known model sensitivities. Its performance may vary depending on the input data quality and the specific characteristics of the study area. SEBS requires accurate vegetation parameters to be obtained, especially in agricultural areas where accurate vegetation parameters can be obtained, high-resolution imagery with low sensor zenith angles is available, and canopy cover is complete. This requirement may limit the applicability of SEBS in areas where such data is not readily available (Gibson et al., 2013).

2.2.2 Field-Based CWP Methods

Several field estimation methods can be used to improve CWP, including lysimeter measurement, nuclear techniques, modelling approaches, field observations, and genetic enhancement. Lysimeter measurement and nuclear techniques have been used to improve water management, saving water by reducing the loss of components that are not used by the plants and thus enhancing water productivity (WP) (Abou Zakhem et al., 2019). These techniques involve measuring soil water content, evaporation, and deep percolation to determine the amount of water used by plants and the amount lost to the environment. However, this method is limited at a small scale.

Field observations can also be used to estimate CWP. A study done by (Shoukat et al., 2021) investigated the effects of deficit irrigation and fertilizer levels on wheat crop yield, yield parameters, nutrient use, and water use efficiencies. The study followed a randomized complete block design of three replications, taking three irrigation treatments according to the requirement of crop estimated by the CROPWAT model (100% of ETC), deficit irrigation (80% of ETC), and deficit irrigation 60% of ETC and three nitrophenols fertilizer treatments at different growth stages. A commonly used field method for CWP estimation is the harvest method. The harvest method involves measuring the crop yield and the amount of water used for irrigation, and then calculating the crop water productivity (CWP) as the ratio of yield to water use. This method provides a direct measure of the productivity of a crop in terms of water use efficiency. The method faces limitations of extent especially for large spatial areas, and data availability, especially for the amount of water lost. Field-based methods may not be equally applicable to all crop types as different crops have diverse water requirements, growth patterns, and responses to water. In addition, CWP can change over time due to climate variability, seasonal fluctuations, and other

factors. Field-based methods might provide only a snapshot of CWP for a specific period, limiting their ability to capture long-term trends.

2.2.3 Remote sensing and Machine learning Approaches

Remote sensing is a technique used to estimate crop water productivity by analyzing data collected from a distance, such as satellite imagery. This method has become increasingly popular in recent years due to its ability to support management, monitoring, and controlling activities at different spatial and temporal scales (Dalla Marta et al., 2018). Remote sensing has revolutionized the way we monitor and estimate crop water productivity (CWP) by providing valuable data on crop health, water stress, and environmental conditions over large agricultural areas. With the ability to gather information from satellites, drones, and other airborne platforms, remote sensing techniques have become essential tools for sustainable water management in agriculture. (Li et al., 2008; Talpur et al., 2023, Gao et al., 2023, Spiliotopoulos et al., 2023 and (Darwish et al., 2023) successfully utilized remote sensing technologies in the estimation of crop water use and productivity.

The use of remote sensing indices is utilized to estimate crop water productivity. Commonly used indices include NDVI (Mohanasundaram et al., 2023; Pandya et al., 2023; Farrell et al., 2018), EVI (Jaafar & Ahmad, 2015; (Tang et al., 2015), NDWI (Singh et al., 2021; (Z. Wang et al., 2009) and TVDI (Holzman & Rivas, 2016) and more. NDVI is one of the most widely used remote sensing indices for assessing vegetation health. It quantifies the density of green vegetation and indicates plant Vigor and growth. NDVI values close to +1 indicate healthy, thriving vegetation, while values closer to -1 indicate stressed or sparse vegetation. By monitoring NDVI over time changes in crop water productivity can be inferred. EVI is an improvement on NDVI, designed to reduce atmospheric influences and improve sensitivity at high vegetation densities. It provides a more accurate representation of vegetation conditions, making it suitable for areas with dense vegetation cover or during periods of high atmospheric interference. TVDI combines thermal infrared data with NDVI to assess water stress in crops. It uses the difference between daytime land surface temperature and the potential temperature under non-water-stressed conditions. TVDI is beneficial for monitoring crop water status, especially in regions where water scarcity is a concern.

Machine learning (ML) techniques on the other have been increasingly employed in the agricultural field to improve the accuracy and efficiency of crop water productivity estimation. This technique has proven to be more efficient in crop yield prediction (Ashwitha & Latha, 2022), water demand forecasting (Emami et al., 2022), remote sensing and Image analysis (Thapa et al., 2023), drought monitoring and mitigation, precision Irrigation, and agriculture. Machine learning techniques offer powerful tools to analyse complex datasets, predict crop water requirements, and enhance water productivity in agriculture.

Despite the use of remote sensing and machine learning in crop water productivity estimation, they also have limitations. The limitation may be due to data availability and quality. Remote sensing relies on data from satellites and other sensors, and the availability and quality of this data can vary. Cloud cover, sensor malfunctions, and limited satellite revisit frequency can lead to gaps in data, making it challenging to get consistent and timely information for accurate estimations. Another limitation is spatial and temporal resolution. The spatial resolution of remote sensing data may not be sufficient to capture small-scale variations within fields or individual plants. Similarly, the temporal resolution may not always be high enough to capture rapid changes in crop water needs, especially in rapidly evolving weather conditions. Finally, the complexity of the crop-water relationship poses a major challenge in accurate water productivity estimation. The relationship between crop water productivity and remote sensing parameters is complex and influenced by various factors like crop type, stage of growth, and weather conditions. Capturing these complex interactions in a single model can be challenging.

3. Materials and methods

3.1 Study area

The Bura irrigation scheme is the study area located in Tana River County (1°11'39.1S, 39°50'23.0"E). The scheme is one of the largest and oldest irrigation projects in Kenya. It was established in the 1978s and covers an area of about 12,000 acres gazette area and 10,000 acres under irrigation (National Irrigation Authority, 2023). The primary water source is from River Tana which is 50 km away and maize is the main crop grown in the area. Other crops grown in the area include green grams, cowpeas, cotton, watermelon, sugarcane, and onions.

Low and erratic rainfall patterns characterize the scheme. The average annual rainfall in the region is relatively low, ranging from 200 to 600 millimeters (8 to 24 inches). This results to an average of about 400mm of rainfall in the region (Muigai David et al., 2019). The rainfall is highly variable, with the most precipitation occurring during the short rainy season from March to May and a shorter second rainy season from October to December (Mbayaki, 2021). Drought periods are standard, and rainfall distribution can vary significantly from year to year.

Due to the arid conditions, evapotranspiration rates are relatively high in the Bura irrigation scheme. High temperatures and low humidity contribute to increased evapotranspiration rates, which can impact water availability for crops.

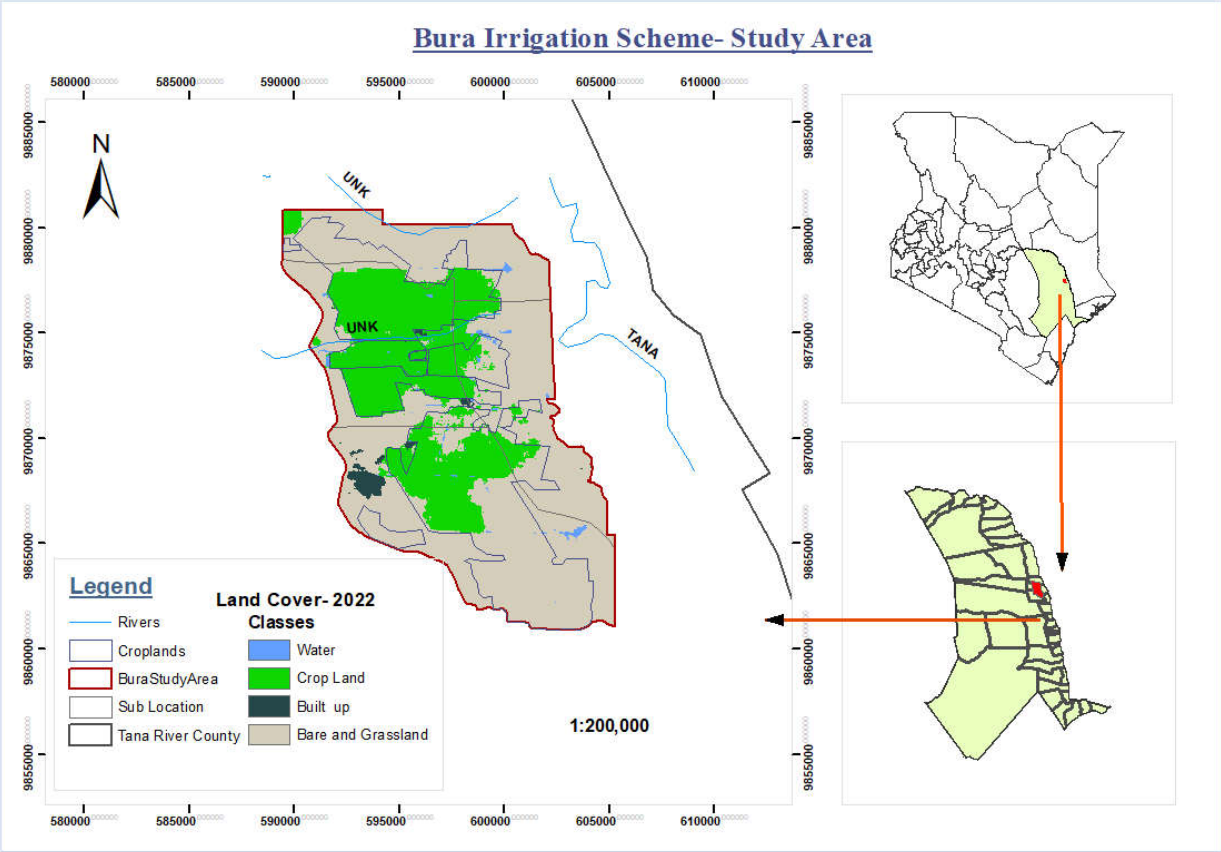

Figure 3.1: Study area map

3.2 Data

This study utilizes both remote sensing and ground-based data for both crop yields and climate-related data. Remote sensing data were acquired from the Google Earth Engine using Python API for five years between 2018 and 2022 with the main focus being during the growing seasons.

3 .2.1 Meteorological Data

The availability of consistent, long, and complete time series of meteorological data is critical for estimating crop water requirements because weather is the most important input variable for assessing crop evapotranspiration which determines soil water deficit. This study used the ERA5 daily Grided dataset accessible from the GEE catalogue and the local meteorological station dataset. ERA5 is the fifth generation ECMWF reanalysis of the previous eight decades' worth of global climate and weather data. Data is accessible beginning in 1940 to date (Copernicus, 2018). The dataset contains basic atmospheric meteorological factors such as air temperature, pressure, and wind at various altitudes, as well as surface parameters such as rainfall and sea parameters such as sea-surface temperature and wave height. The daily homogenized, filtered, reviewed, and pre-processed (outliers removed) data of minimum temperature (Tmin), maximum temperature (Tmax), mean temperature (Tmean), Precipitation, incoming solar radiation, vapor pressure, and wind speed (u -component at 10m high above the ground) were acquired from Google Earth Engine (GEE) data catalogue for a period of five years; between 2018 to 2022. In the case of vapor pressure, the information may not be directly available in the ERA5 dataset. However, it was estimated using atmospheric parameters such as air temperature and relative humidity as previously implemented by (Pelosi et al., 2022) on crop water requirement studies.

Similarly, daily weather data for the Garissa weather station was acquired from the Kenya Meteorological Department on request. This was for the same period and it was used as part of the ground validation data together with the actual ground yield data. More accurate data could be acquired at the exact field level and in several locations but this was limited in this study.

3.2.2 Optical Satellite Imagery Datasets

In this study, several optical datasets were acquired from the GEE platform, including MODIS, Landsat 8, and Sentinel 2 datasets. MODIS provided high temporal resolution data of up

to daily with an average 8-day temporal resolution being provided. Three surface reflectance products were used for the purpose of data fusion. In this case, MOD09A1.061 Terra Surface Reflectance 8-Day Global 500m product, USGS Landsat 8 Level 2 Collection 2 Tier 1 and Sentinel-2 MSI Multi spectral Instrument Level-2A dataset were accessed from the GEE data catalog using Python API. Landsat 8 dataset has a spatial resolution of 30m, and sentinel 2 has the B2 - B4 and B8 having a spatial resolution of 10m. To achieve a harmonized resolution, resampling was performed on the datasets to achieve a 10m spatial resolution. Table 3.1 below summarizes the data used in this study.

Data	**Description/Resolution**	**Source**
Temperature (Tmin, Tmax), Incoming Solar radiation, vapor pressure, Wind speed, and Precipitation	From ERA5_L and Daily Dataset and Actual Meteorological Local Station Data.	ECMWF/ KMD (Kenya Meteorological Department)
Soil Moisture	1-Month	GLDAS
Evapotranspiration (ET)	8-Days at 500m resolution	MODIS
Surface reflectance (Derived Dataset: NDVI, SAVI, EVI, etc.)	10m - Fused dataset	Sentinel 2, Landsat 8 OLI, MODIS

Table 3.1: Datasets used

3.3 Methodology Flowchart

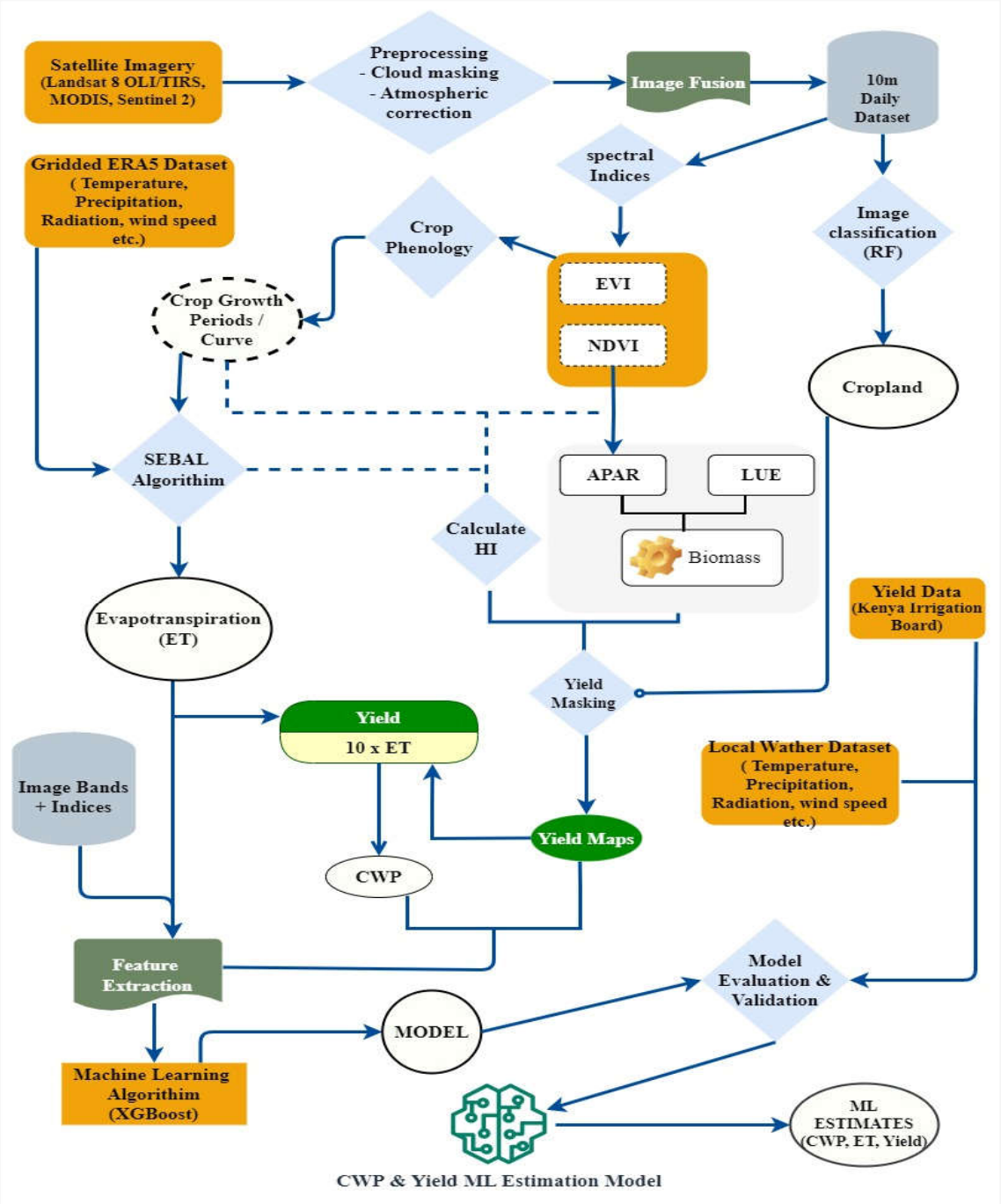

Figure 3.2: Flowchart

3.4 Data Fusion and Indices Calculation

3.4.1 Daily Imagery Dataset

The increased availability and diversity of global satellite products, as well as the rapid development of new algorithms, has opened up huge opportunities for the creation of new levels of data with varied geographical, temporal, and spectral resolutions (Dhillon et al., 2023). MODIS has a short return interval, and the data quality is consistent. However, because of the limited spatial resolution, it isn't applicable to the small-scale region. Sentinel-2 and Landsat 8 data have a better spatial resolution of about 10m and 30m lowest value for some bands than MODIS data, although the data quality is unreliable.

The implementation of the fusion algorithm for the three datasets was based on a method implemented by (H. Gao et al., 2023) by extending the formula used with one for Landsat. However, several fusion algorithms do exist. An example is the improved spatial and temporal data fusion approach (ISTDFA) used by (Wu et al., 2018) to fuse MODIS and Landsat. Another algorithm used was STAIR 2.0 for the fusion of MODIS, Sentinel 2, and Landsat. Similar other common algorithms are the Spatial and Temporal Adaptive Reflectance Fusion Model (STARFM) and two extended data fusion models (STAARCH and ESTARFM) that have been used to fuse MODIS and Landsat data (F. Gao et al., 2015). In this study, the fusion algorithm utilized the formula provided below to obtain a daily 10 m resolution dataset.

$$V_H(t_i) = V_M(t_i) + K.\frac{\sum_{j=1}^{n}\left[\omega(t_i,t_j)\left(V_T(t_j) - V_M(t_j)\right)\right]}{\sum_{j=1}^{n}\omega(t_i,t_j)} + K.\frac{\sum_{k=1}^{m}\left[\omega(t_i,t_k)\left(V_L(t_k) - V_M(t_k)\right)\right]}{\sum_{k=1}^{n}\omega(t_i,t_k)} \quad (1)$$

$$\omega(t_i, t_j) = \frac{1}{|t_i - t_j| + 1} \quad (2)$$

$$\omega(t_i, t_k) = \frac{1}{|t_i - t_k| + 1} \quad (3)$$

Where:

- $V_H\ (t_i)$ - Value of the fused image pixel at time t_i
- $V_M\ (t_i)$ - Value of the MODIS image pixel at time t_i
- $V_T\ (t_j)$ - Value of the Sentinel-2 image pixel at time (t_j)
- $V_L\ (t_k)$ - Value of the Landsat 8 image pixel at time t_k
- N - Number of Sentinel-2 images
- M - Number of Landsat 8 images
- t_i - Day of Year (DOY) corresponding to the MODIS data.
- t_j - DOY corresponding to the Sentinel-2 data
- t_k - DOY corresponding to the Landsat 8 data.
- $\omega\ (t_i, t_j\ )$ - Weight of the Sentinel-2 image at time t_i, t_j
- $\omega\ (t_i, t_k\ )$ - Weight of the Landsat 8 image at time t_i, t_k
- K - Empirical coefficient accounting for the influence of missing Sentinel-2 and Landsat 8 images on data fusion.

The fusion process involved data preprocessing like performing atmospheric corrections on the Landsat 8 images, and Sentinel 2 images. Cloud masking and filtering were performed to ensure that cloud-free images are obtained for fusion. This methodology adopted a procedure utilized by (Luo et al., 2020) in the actualization of the STAIR 2.0 algorithm. This involved cloud removal, and resembling for MODIS dataset from 500m to 30m spatial resolution and fusing MODIS with Landsat as shown in equation (1) above. Similarly, atmospheric corrections, co-registration, and cloud removal and filtering were performed on the Sentinel-2 dataset which was then fused with resampled 10 m resolution MODIS-Landsat 8 dataset to 10 m resolution daily dataset collection between 2018 to 2022.

Figure 3.2 shows a sample NDVI map comparing the output from the fused dataset and coarse 500m resolution MODIS NDVI for the period between January and December 2022. This help to achieve both high spatial and temporal resolution for the fused dataset to ensure improved crop monitoring and metric generation within the study area.

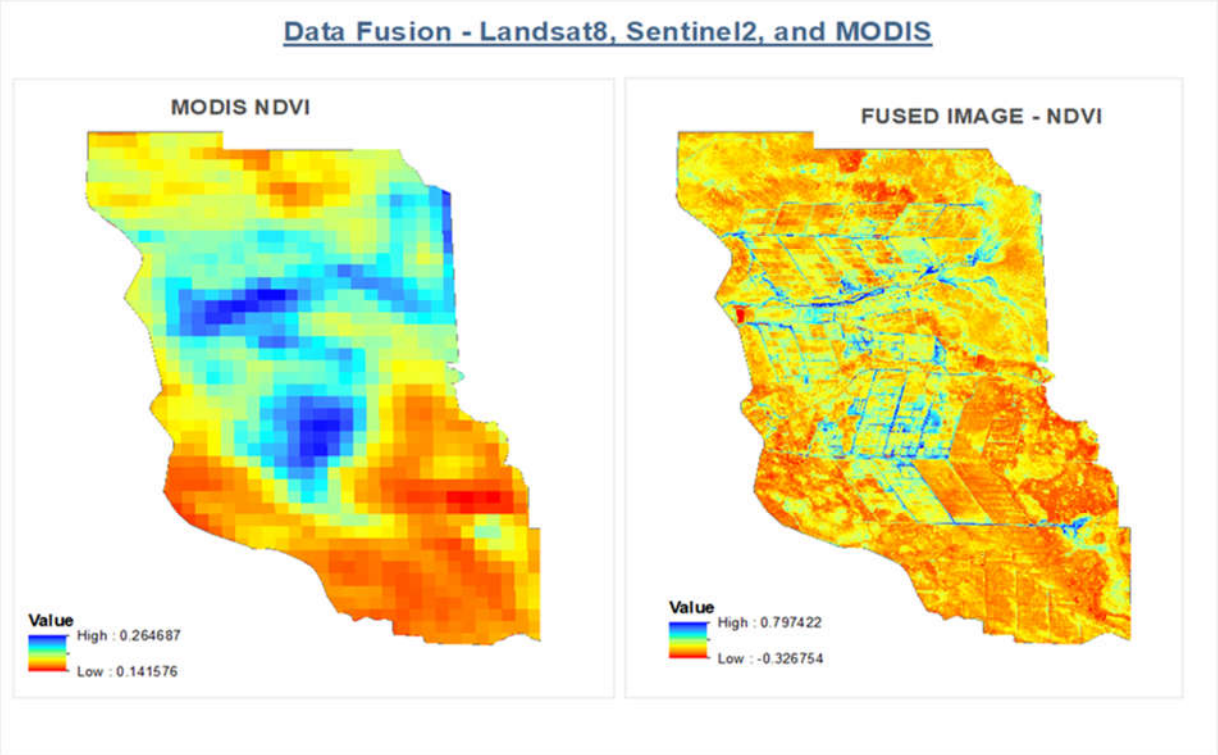

Daily data NDVI comparison

3.4.2 Indices

The study calculated several indices to support the analysis of CWP and machine learning modeling. The indices are drought-based, vegetation-based, soil-based, and water-based. They include NDVI, VCI, and more.

Table 3.2 below summarizes all the indices calculated and used in the study.

Indices	**Expression**	**Use Case/ Reference**
NDVI	(NIR - Red) / (NIR + Red)	(Dhau et al., 2021; Bolfe et al., 2023)
EVI	2.5 * ((NIR - Red) / (NIR + 6 * Red - 7.5 * Blue + 1))	(Dhau et al., 2021)
GNDVI	(NIR - Green) / (NIR + Green)	(Dhau et al., 2021)
MSAVI	(2 * NIR + 1 – sqrt ((2 * NIR + 1) ^2 - 8 *	(Dhau et al., 2021)

	(NIR - Red))) / 2	
MNDWI	(Green- SWIR)/ (Green + SWIR)	(Agilandeeswari et al., 2022; Laonamsai et al., 2023)
EDI	(PET - ET) / PET	(Khan et al., 2018)
VCI	(NDVIi - NDVImin)/(NDVImax - NDVImin)	(Sánchez et al., 2016; Zhao et al., 2022)
TCI	(LSTmax - LSTi)/(LSTmax - LSTmin)	(Sánchez et al., 2016; Zhao et al., 2022)
SMCI	(SMi - SMmin)/(SMmax - SMmin)	(Sánchez et al., 2016; Zhao et al., 2022)

Table 3.2: Spectral indices

3.5 Crop Yield

Yield calculation in this study is achieved by determining total dry matter biomass and harvest index. Harvest index is a key agricultural term that relates to crop plants capacity to convert photosynthetically fixed carbon into edible yield which is frequently the crop's harvested component such as grains, fruits, or vegetables. Combined product of harvest index and summation of biomass results to yield estimate. In this case, the Biomass-Harvest index method is used. The harvest index method is inherited from a study by (Moriondo et al., 2007).

$$HI = HI_{max} - HI_{.range}\left(1 - \frac{NDVI_{POST}}{NDVI_{PRE}}\right) \quad (4)$$

Where:

HI - Actual Harvest index for C4 crop (maize/corn)

HI_{max} - Maximum harvest index for maize. In C4 crops have been chosen to be 60% (0.6)

HI_{range} - The range selected is 0.2 for C4 crops.

$NDVI_{POST}$- The mean value of NDVI between flowering and maturity

$NDVI_{PRE}$- The mean value of NDVI between planting and flowering for maize crop.

Dry matter Biomass estimation utilizes NDVI values and solar radiation as major input parameters. According to Bastiaanssen & Ali, 2003, Biomass can be estimated using the following formula.

Biomass = Σ (0.864 x ε x APAR) (5)

Where:

ε is the light use efficiency (LUE) and APAR is the 24-hour absorbed photosynthetically active radiation (W/m^2). APAR is given as shown;

APAR = 0.48 x f x S↓ (6)

Where f refers to the APAR fraction which changes with respect to the leaf area index. S↓ Represents the incoming solar radiation. This component is obtained from weather data. The value of 0.48 is an average or typical value that has been found to represent the efficiency of plants in converting PAR into chemical energy through photosynthesis. It is also important to note that the PAR value describes the total amount of radiation available for photosynthesis assuming leaves intercept all sunlight. This is a very speculative estimate since leaves both transmit and reflect solar radiation.

Determination of the fraction of APAR (f) depends on vegetation indices of the crop at a specific point in time. In this case, NDVI is specifically used as the main index in the calculation of the fraction of APAR. Given by the expression;

$$f = -0.161 + 1.257\ NDVI_t \quad (7)$$

Another important component used in the determination of Biomass is the LUE. LUE quantifies the plants' *efficiency* in utilizing solar radiation for photosynthetic carbon fixation. Given by the expression;

$$\varepsilon = \varepsilon_{max} \text{x g(T) x g(D) x } \lambda \quad (8)$$

ε_{max} represent the max value for C4 crops like corn/maize. A study determined ε_{max} to be approximately 2.5 gMJ^{-1} (Huang et al., 2022). Similarly, g(D) accounts for vapour pressure, and g(T) accounts for crop heat stress. Both g(T) and g(D) and scalar quantities. Finally, λ represents the water stress mainly obtained as an evaporative fraction.

Utilizing results from biomass and harvest index (HI), yield is then obtained by the following expression;

Yield (Y) = Biomass x HI (9)

3.6 Evapotranspiration Estimation

The estimation of actual ET utilizing the SEBAL algorithm parameters was achieved by the following formular which is based on thermal and multispectral remote sensing datasets that compute latent heat flux (LE) as a residual by subtracting the soil heat flux and sensible heat flux from the instantaneous surface energy balance equation's net radiation (Rn) (Gonçalves et al., 2022). In the computation of ET, both weather data and satellite images are used. LE is expressed as shown in equation (10).

LE = Rn - G - H (10)

Where H is the instantaneous sensible heat flux (W/m^2), and G is the soil heat flux (W/m^2). Furthermore, Rn and G are determined as follows;

Rn = (1 - α) Rs↓ + R*l*↓ - R*l*↑ - (1 - ε_0) Rl↓ (11)

$$\frac{G}{Rn} = \alpha(T_S - 273.15)\,(0.0038\alpha + 0.0074\alpha^2)(1 - 0.98\mathrm{NDV}l^4) \quad (12)$$

Where α is the surface albedo calculated from satellite image bands according to (Tasumi et al., 2008) that demonstrated this using landsat image bands. Rs↓ represent the incoming short-wave radiation, R*l*↓ is the incoming long wave radiation, Rl↑ the outgoing longwave radiation, and ε_0 is the surface thermal emissivity. According to (Jaafar & Ahmad, 2020), Ts, corr is the corrected land surface temperature (Ts) in K based on the DEM map and the difference between extraterrestrial solar radiation on sloping and flat terrains to account for temperature variations owing to common elevation data and slope.

The automated statistical technique used to choose the hot and cold endmembers is a reduced version of the CIMEC algorithm used in METRIC. Endmember candidates are chosen based on percentiles of LST and normalized difference vegetation index (NDVI) readings. To calibrate the dT function, the CIMEC process is employed. Surface temperature, wind speed, surface roughness, and surface-to-air temperature gradients are all used to determine sensible heat flow (H).

$$H = \frac{\rho_a Cp dT}{r_{ah}} \quad (13)$$

Where Cp is the specific heat capacity and r_{ah} is the aerodynamic resistance of turbulent heat transport from the evaporating surface at height z1 to the air above the evaporating surface z2. To solve the iteration process, it is necessary to select hot and cold endmembers. In this case linear relationship between T_S and (dT) is assumed; a and b coefficients are empirically determined for each image.

$$dT = a + bT_S \quad (14)$$

More details from research paper done by Laipelt et al., 2021.

The evaporative fraction (Λ) is expressed as

$$\Lambda = \frac{LE}{Rn - G} \quad ; \quad (16)$$

To obtain daily ET, the following expression is used within the SEBAL algorithm.

$$ET_{a24h} = \frac{\Lambda R_{n24}}{\lambda} \quad (16)$$

where λ is the latent heat of vaporization (MJ·kg-1).

In addition, the maize crop coefficient was calculated utilizing the Penman-Monteith equation (Wang et al., 2023) which is recommended by FAO. ETa is given by the expression;

$$ET_a = ET_0 \times K_c \quad (17)$$

ET_0 is the daily potential evapotranspiration and K_c is the crop coefficient for maize at the corresponding growth stage.

$$ET_0 = \frac{0.408\Delta\,(Rn - G) + \gamma \frac{900}{T_{mean}+273} u_{10}\,(e_s - e_a)}{\Delta + \gamma\,(1 + 0.34\,u_{10})} \quad (18)$$

Where Δ represent the slope of saturation of water pressure curve, T_{mean} is the mean of daily air temperature at 10m height in degrees celsius, u_{10} is the speed of wind at 10m height in meters per second, e_a represent the actual vapour pressure and e_s is the saturation vapour pressure. The difference of e_s and e_a gives the saturation vapour pressure deficit. γ is the psychrometric constant. Rn, and G is as previously defined. More on the calculation of each component fellows (Gebremedhin et al., 2022).

Crop coefficient (Kc) is spatially and temporary variable depending on the crop type and the stage of growth. The determination of Kc values followed expressions documented by (Cemek et al., 2023). The combination of ETa and ETo is therefore used to determine the correlation between Kc and NDVI withing the study area. According to FAO, Kc values ranges from 0.2 to 1.2 with the following periodic breakdown; initial stage, crop development stage, mid development stage and late stage.

3.7 Crop Water Productivity

CWP then estimated using crop determined yield (Equation 9), and crop evapotranspiration (Equation 16). Yield units being in kilograms per meter squared (kg/m^2) and evapotranspiration units being m^3/m^2. Water productivity maps were created by dividing agricultural production maps by water use maps. The expression for CWP is as shown in equation 19.

$$CWP = (Yield\ (Y)) / (10 \times ETa_{mean}) \quad (19)$$

where ETa_{mean} is the mean actual evapotranspiration over the growing period when the estimation is performed

4. Results

4.1 Crop Phenology

Study regarding crop growth stages is determined based on the cover characteristics within the study area. Using the NDVI and EVI, average growth period was analysed and the resultant curve shows the dates of each stage. Figure 4.1a and Figure 4.1b provides a graphical presentation of the vegetation growth characteristics with respect to the specific day of the year. The continuous alignment of NDVI and EVI curves throughout reveals their significant association, emphasizing their importance in crop phenology assessment. This agreement emphasizes the durability and dependability of these vegetative indicators, reaffirming their importance.

Two main growth seasons were identified as long season and short growing season. Short season ranges between DOY -220/270 to 355 (August/September to December). The long season happens DOY-410 to 605 (late January to August). This was found to agree with planting periods as outlined in other studies within the study area (Muigai David et al., 2019) . A window of 1 to 2 weeks is applied to these growth stages to ensure that it captures the differences that may arise within the Irrigation scheme.

The sowing period shows some discrepancy from what could happen in areas with completely reliance on rainfed agriculture. The study area being an irrigation scheme, the sowing period does not start completely from zero NDVI or EVI index value as it could be in rainfed areas. This is a contribution by factors such as crop rotation, continuous crop alternation within the crop growth stages. This implies that both sowing and maturity of maize crop happen concurrently within the study between DOY – 345 (Maturity) and DOY – 405 (sowing).

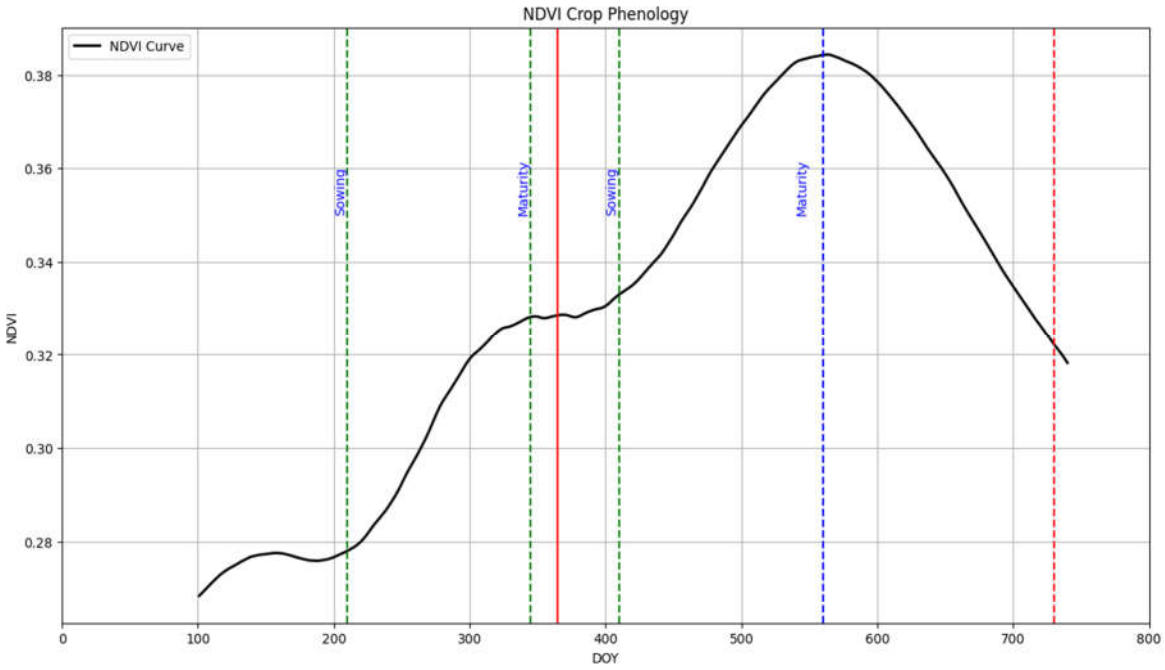

Figure 4.1a Crop growth curve

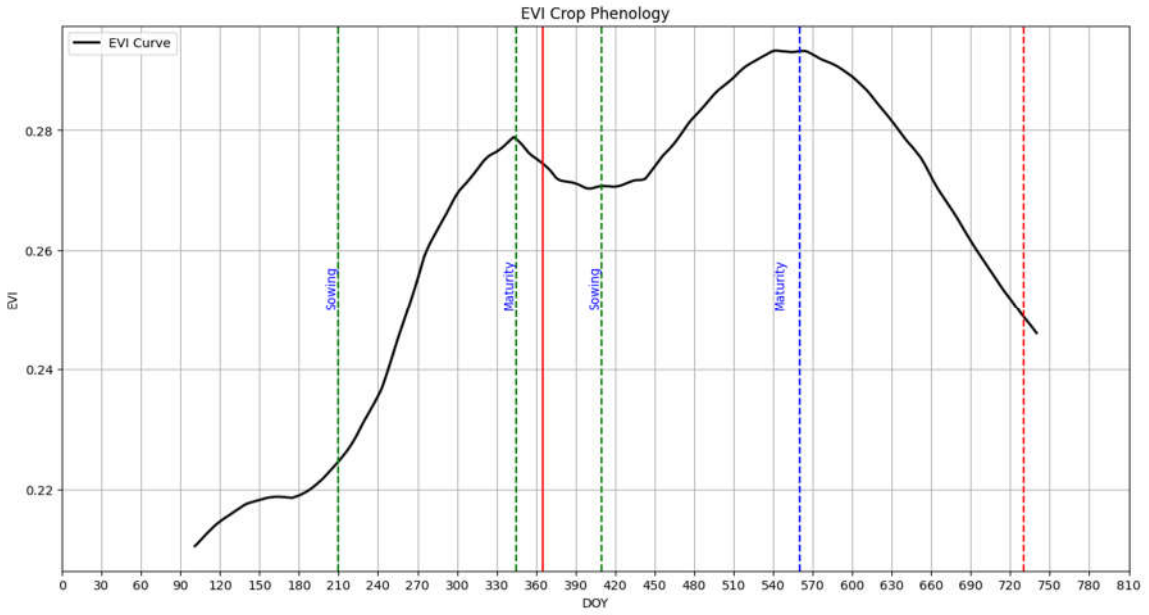

Figure 4.1b Crop growth curve

4.2 Yield Estimation

4.2.1 Classification

The land cover classification, accomplished through Random Forest analysis, successfully identified six distinct classes: bare land, tree cover, grassland, maize, other crops, and water bodies. The classification results exhibit a high degree of accuracy, enabling precise delineation and monitoring of land use patterns.

Table 4.1 shows the error matrix for classification using random forest for the year 2022.

Table 4.1: Classification error matrix

Crop land delineation is achieved through classification with main goal of using the maize crop land for masking other layers of land pattern. The supervised classification using random forest performed well in mapping tree cover, maize, and water. The three classes have an accuracy of above 85; both user and producer accuracy.

Thes classification was then applied on yearly basis between 2018 to 2022 to determine cropland pattern in the study area. Figure 4.2 below shows the classification map for the year 2022.

Classification	Reference								
		Grassland	**Tree Cover**	**Maize**	**Other Crop**	**Bare Land**	**Water**	**Row Total**	**User's Accuracy**
	Grassland	0.198	0.007	0.163	0.151	0.002	0.007	0.527	37.60%
	Tree Cover	0.014	82.283	1.442	0.055	0.194	0.015	84.003	98.00%
	Maize	0.201	0.339	11.005	0.023	0.141	0	11.71	94.00%
	Other Crop	0.024	0.005	0.05	0.456	0.02	0.023	0.578	78.90%
	Bare Land	0.001	0.089	0.149	0.113	0.568	0.001	0.92	61.70%
	Water	0.001	0.063	0.011	0.004	0.001	2.181	2.262	96.40%
	Column Total	0.439	82.786	12.82	0.803	0.925	2.227	**Overall Accuracy: 96.7%**	
	Producer's Accuracy	**45.10%**	**99.40 %**	**85.80 %**	**56.80 %**	**61.40 %**	**97.90 %**	**Kap: 0.886**	

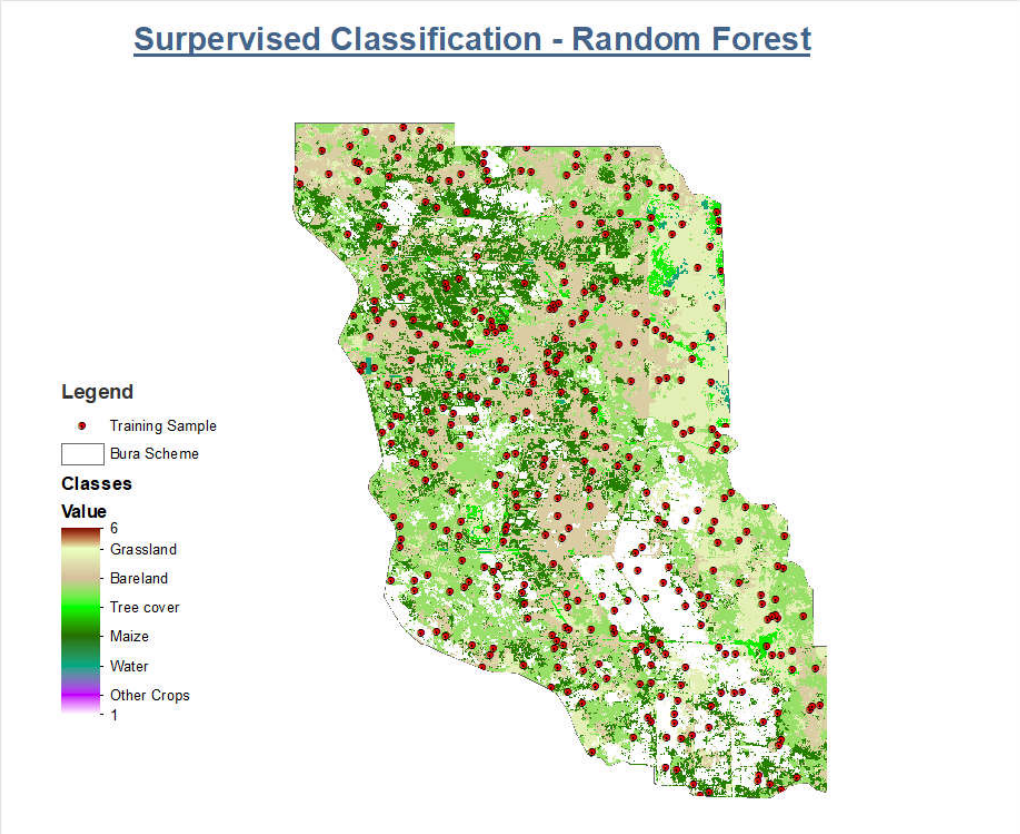

Figure 4.2 Land cover map

4.2.2 Vegetation distribution

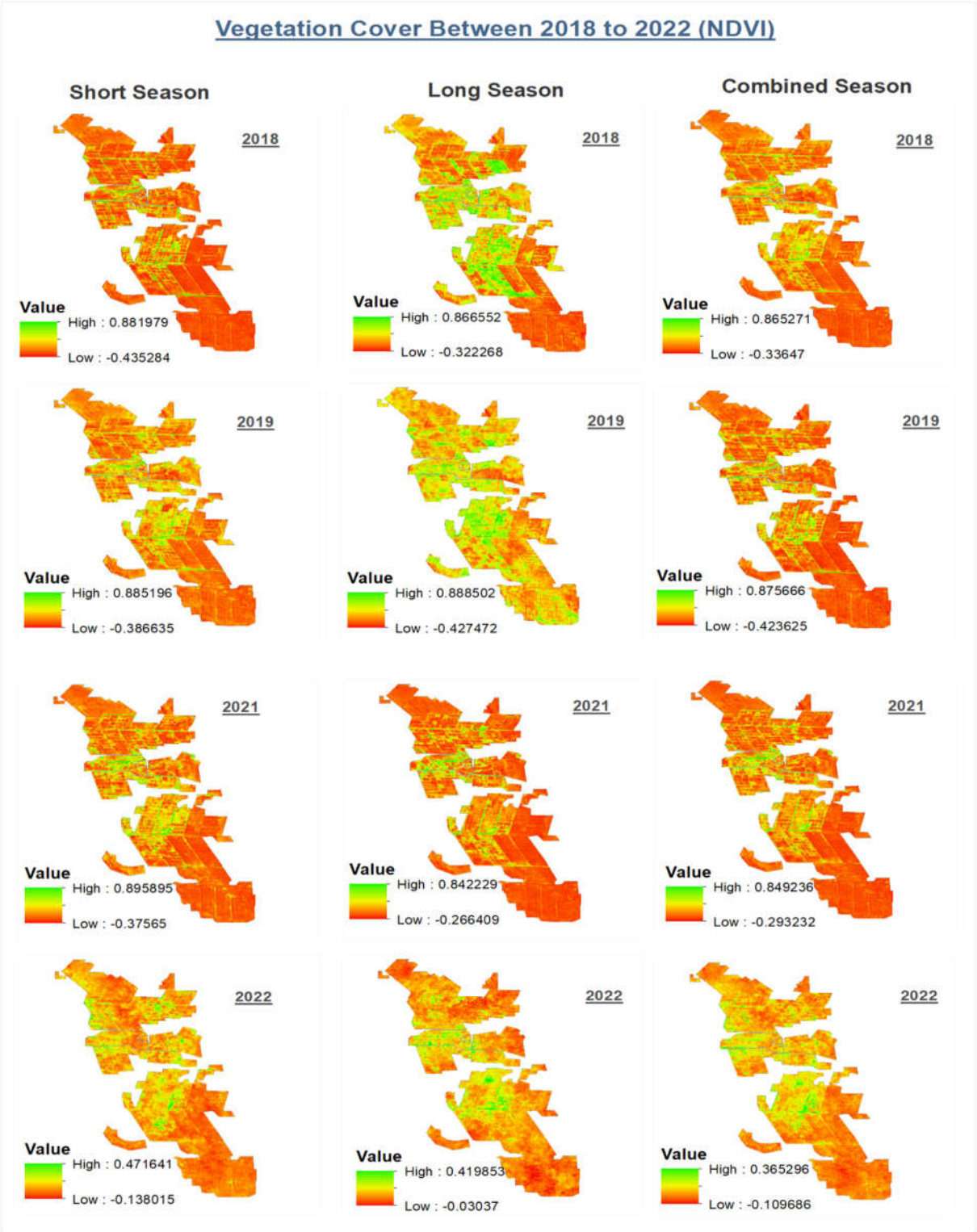

Figure 4.3: Vegetation cover

The Normalized Difference Vegetation Index (NDVI) maps in figure 4.3 above were generated for both short and long growing periods and combined periods over four years (2018, 2019, 2021, and 2022) as part of this study on crop water productivity estimation for resilient agriculture. NDVI is calculated from remote sensing reflectance data and provides an indicator of vegetation greenness and health.

The NDVI maps allow for spatial and temporal analysis of vegetation conditions. Comparing NDVI values across the different growing periods and years provides insights into crop productivity and crop water use efficiency. Higher NDVI values generally indicate healthier, greener vegetation and higher photosynthetic activity. Lower NDVI values may indicate water stress, poor fertility, or other factors limiting plant growth.

The NDVI values vary between the short and long growing periods each year due to differences in crop phenology and water availability. During short growing periods, crops may not reach full canopy cover before the end of the season, resulting in lower overall NDVI. In long growing periods, crops have more time to mature and develop dense, green canopies, leading to higher NDVI values. Finally, the combined season provide the preview of all the seasons image merged to one.

4.2.3 Seasonal Yield Distribution

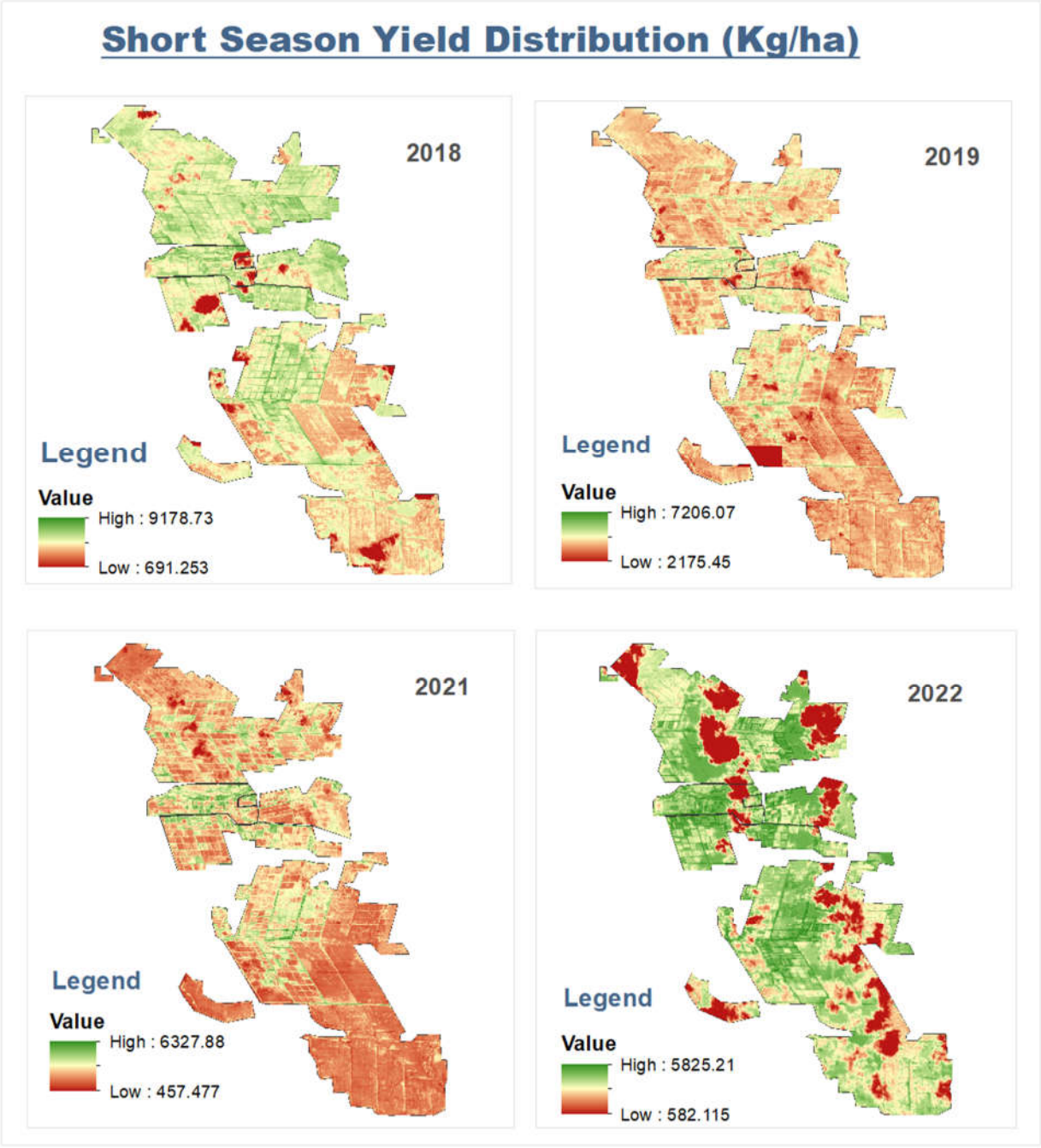

Figure 4.4a: Short Season Yield Estimates map

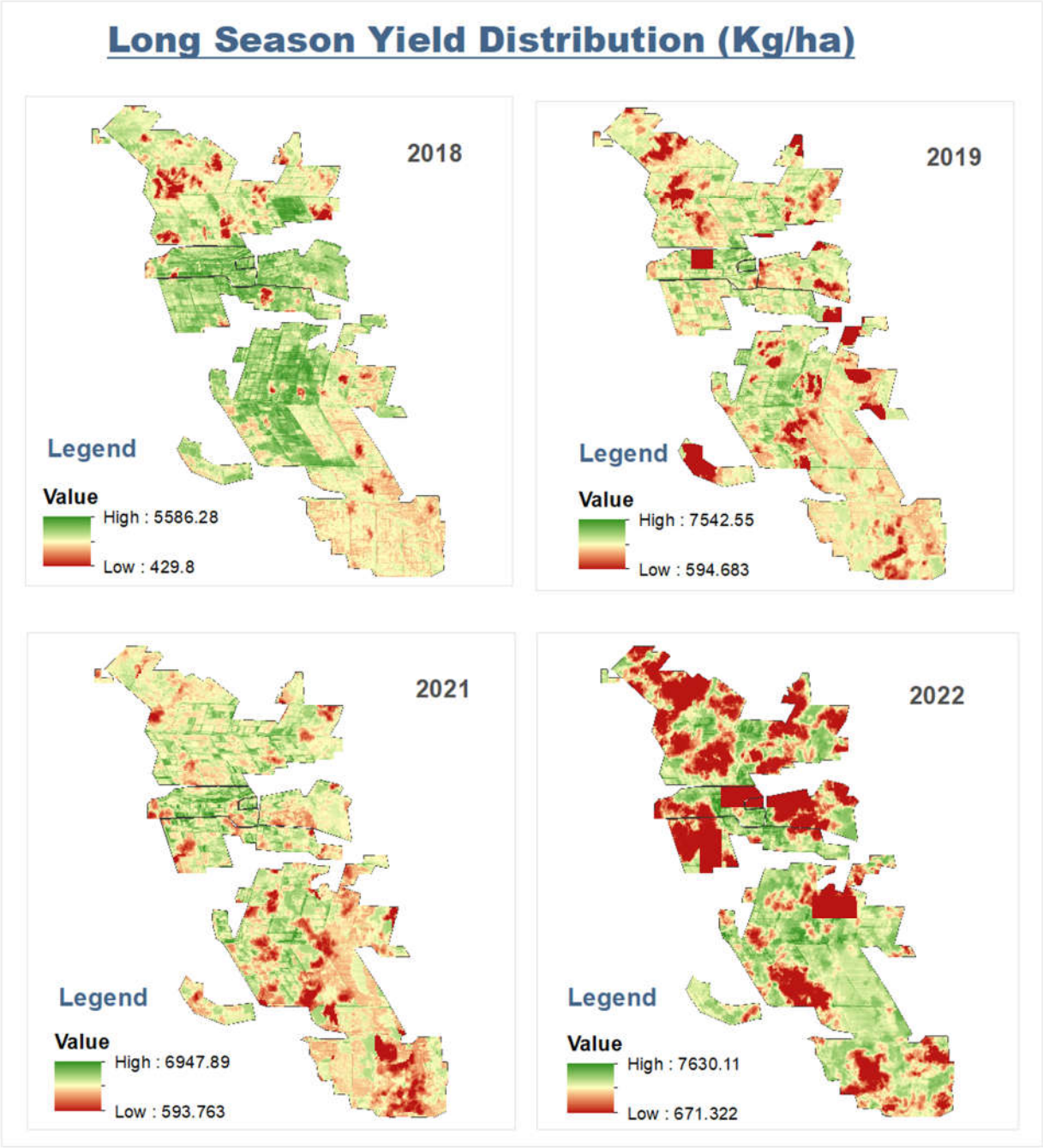

Figure 4.4b: Long Season Yield map.

The crop yield mapping from 2018-2022 revealed clear spatial and temporal patterns in crop production across the Bura Irrigation Scheme. The yield estimates were derived by combining remotely sensed NDVI data with a light-use efficiency model together with APAR to estimate biomass, which was converted to yield using crop-specific harvest index (HI).

For the short growing seasons, yield ranges showed high variability, with minimum yields as low as 457 kg/ha in 2021 and maximum yields up to 9178 kg/ha in 2018 (Fig. 4.4a). The lowest yields tended to be concentrated in the northern and southern parts of the scheme. The 2019 season had the highest overall yields, while 2021 had the poorest yields, likely due to weather fluctuations.

The long growing seasons showed less variability, with minimum yields between 429-671 kg/ha and maximum yields of 5586-7630 kg/ha (Fig. 4.4b). The lowest yields occurred primarily in the southern areas of the scheme. The highest yields were found in the northeast region. Overall, the long-season yields were higher and more stable than the short seasons.

The maps reveal substantial spatial heterogeneity in crop yields, highlighting areas of low crop water productivity. While irrigation supports cropping in this ASAL region, water distribution and drainage issues may be limiting yields in certain parts of the scheme. The temporal variability highlights the impacts of changing weather patterns as well as differences in cropping patterns and management.

In addition to the spatial yield maps, average crop yield was calculated for the entire Bura Irrigation Scheme region for each growing season and year. For the short seasons, average yield ranged from 3.12 t/ha in 2022 up to 5.05 t/ha in 2020 (Table 4.1) below. The long season average regional yields were lower, varying from 3.22 t/ha in 2022 to 3.76 t/ha in 2019. Combined total average yield accounting for both seasons fluctuated between 6.34 t/ha in 2022 and 8.68 t/ha in 2020. The combine yield was obtained as a sum of all the seasons yield in that specific year. To visualize the trend of yield production at regional level within Bura scheme, a bar graph was generated for the same results (Figure 4.5) below.

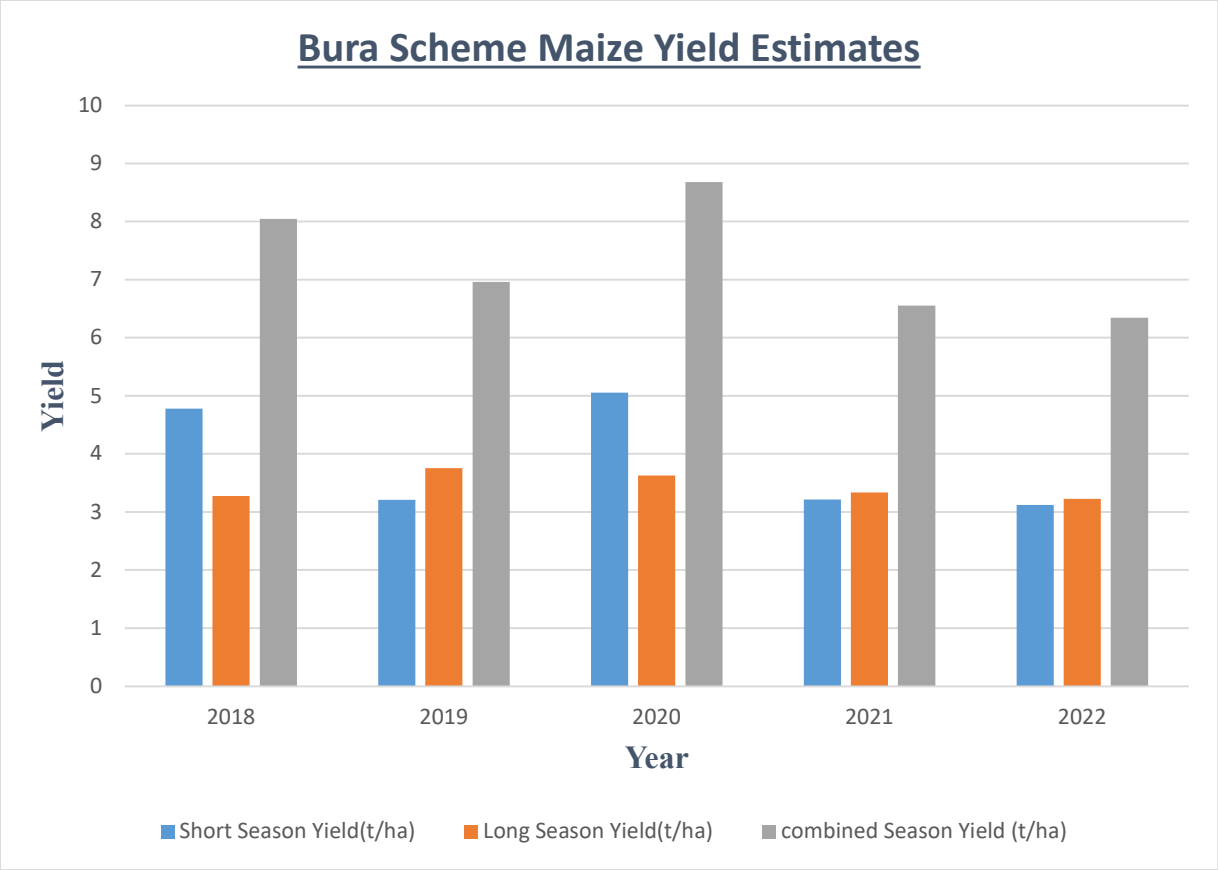

Figure 4.5: Yearly maize yield bar graph

Year	Short Season Yield(t/ha)	Long Season Yield(t/ha)	Combined Season Yield (t/ha)
2018	4.776366357	3.271972696	8.048339053
2019	3.207342922	3.7555	6.962842922
2020	5.052628943	3.626553298	8.679182241
2021	3.215566055	3.336088949	6.551655004
2022	3.121359342	3.222519736	6.343879078

Table 4.1: Yield Data

4.3 Regional Evapotranspiration Estimates

Evapotranspiration (ET) was estimated for the Bura Irrigation Scheme study area from 2018 to 2022 using the SEBAL algorithm and Penman-Monteith equation. During the short growing season (Figure 4.6), ET ranged from a minimum of 9.3 mm to a maximum of 117.0 mm in 2018 with an average of 63.2 mm across the study period. In 2019, the range was wider, from 24 mm to 143.5 mm, with an average of 80.8 mm. The minimum ET stayed consistent in 2021 and 2022 at 9.3 mm, while maximum values were 119.0 mm and 112.0 mm respectively. Average ET for 2021 was 64.2 mm and 61.0 mm for 2022.

For the long growing season (Figure 4.7), minimum ET was 9.3 mm in all years from 2018 to 2022. Maximum ET reached 118.0 mm in 2018, 76.1 mm in 2019, 114.5 mm in 2021, and 143.9 mm in 2022. The average ET for the long season was 73.3 mm in 2018, 42.7 mm in 2019, 62.4 mm in 2021, and 78.6 mm in 2022. Overall, ET was lower and had a narrower range during the short growing season compared to the long season.

The year with the highest ET estimates in the short season was 2019, with an average of 80.8 mm and maximum of 143.5 mm. For the long season, 2022 had the highest ET with an average of 78.6 mm and maximum of 143.9 mm. The lowest ET for both seasons occurred in 2019, with an average of 42.7 mm in the long season.

Higher ET in a particular season and year indicates increased crop water use and demand. Years with higher ET likely experienced better growing conditions, less water stress, and higher potential crop yields. Lower ET suggests crops were more water-limited, leading to reduced productivity. For example, the high ET in 2019's short season suggests crops had adequate moisture while the low ET in the long season indicates water stress.

ET estimates from the two models were relatively consistent, indicating reliable results. Some variability between years can be attributed to changing weather patterns influencing factors like rainfall, temperature, wind speed which affect ET. Overall, these ET maps and estimates provide insights into crop water use over time in the Bura Irrigation Scheme. The data can help inform water management and agricultural decisions to optimize crop productivity.

Figures 4.6 and 4.7 below shows the spatial variability of ET across the scheme.

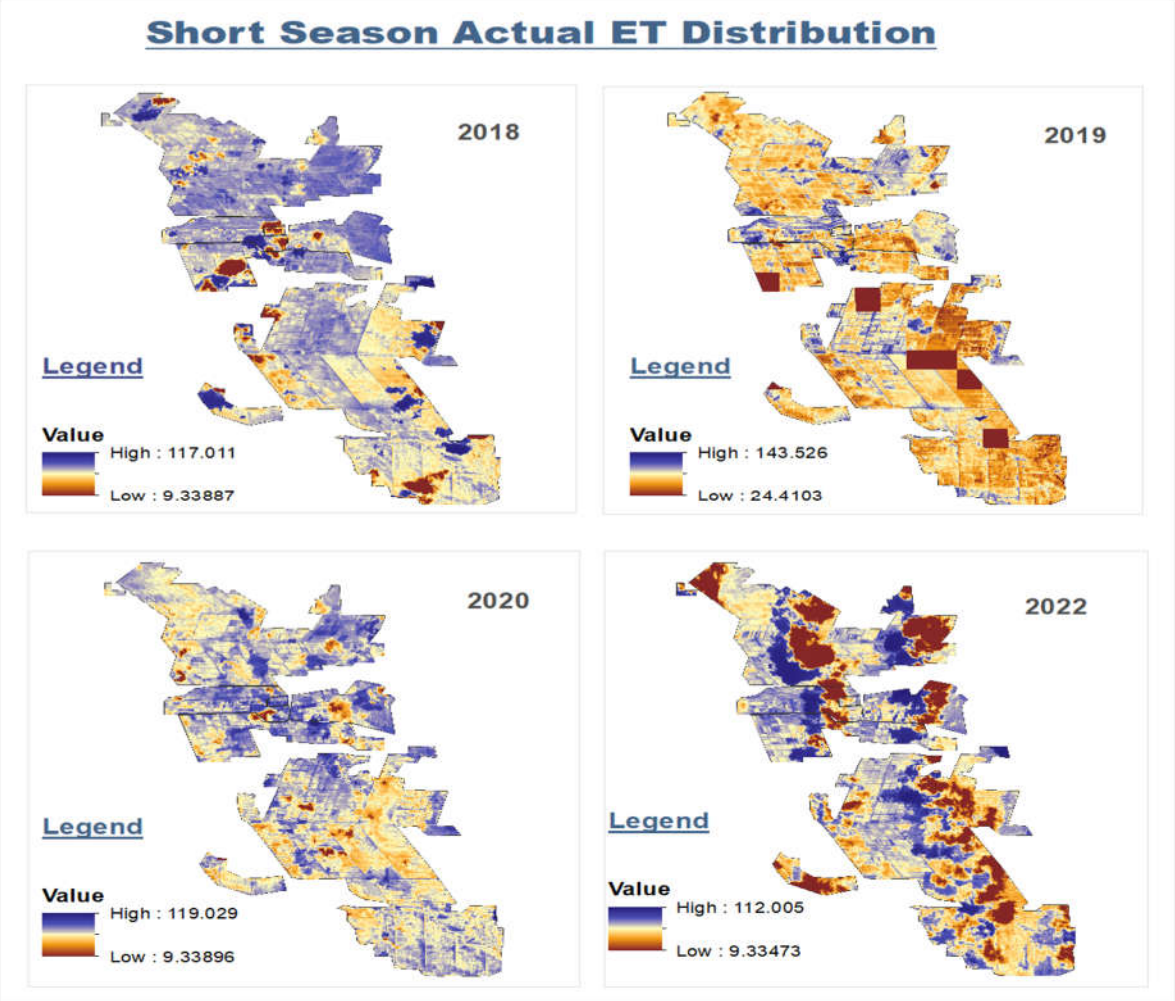

Figure 4.6: 2018 to 2022 short season evapotranspiration maps

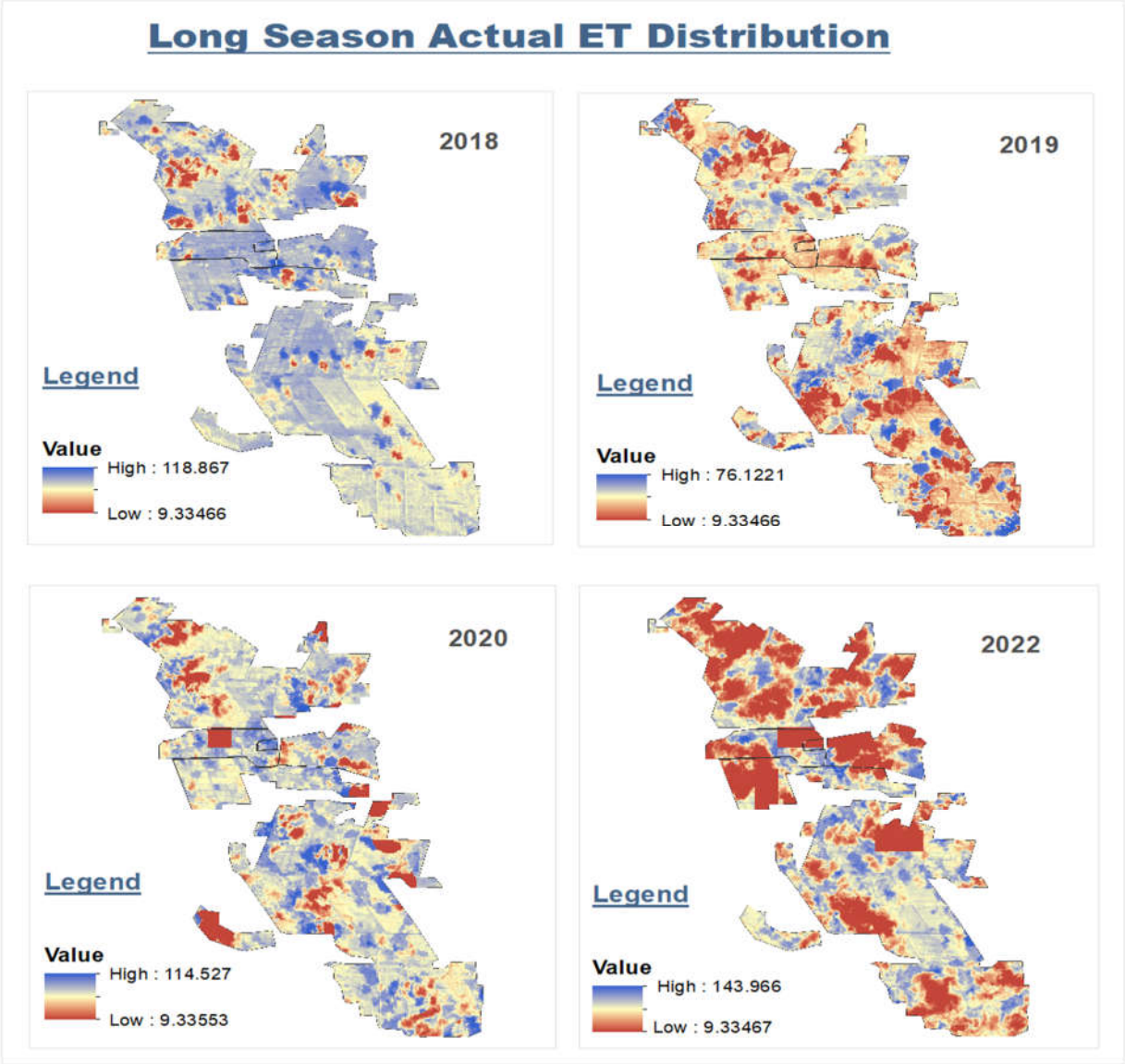

Figure 4.7: 2018 to 2022 long season evapotranspiration maps

4.4 CWP Spatial Distribution

CWP maps is an output based on ET and yield. Its was achieved using Equation 19. Same timeframe and seasons were processed and spatial temporal distribution of CWP maps generated. High values of CWP represent higher productivity while lower values represent lower productivity. Figure 4.8 and 4.9 below shows spatial distribution of CWP between 2018 to 2022 for short and long growing seasons.

Short growing season CWP ranges between a minimum value of 0 kg/m^3 to 10.5 kg/m^3 for the given timeframe. Generally, the southern part of the scheme has low crop water productivity. The central part of the study area has higher CWP which is the main part where irrigation happen. On the other hand, the long growing season CWP was found to range between 0 kg/m^3 to 9.5 kg/m^3. Spatially, CWP was lower in 2022 in most parts of the study area for both seasons. Similar observation can be made in the year 2021 long season and 2019 short growing season. These low CWP results for the stated seasons is as a contribution of high ET with low yields in the maize growing regions.

The crop water productivity maps reveal several important spatial and temporal patterns across the Bura Irrigation Scheme. While the southern areas consistently showed lower CWP, the central and north-western irrigated zones displayed higher productivity that aligned with the intensive agricultural activity in this region. The maps indicate that water management and agronomic practices may need to be re-evaluated in the southern scheme to improve CWP. See Figure 4.8 and 4.9 below.

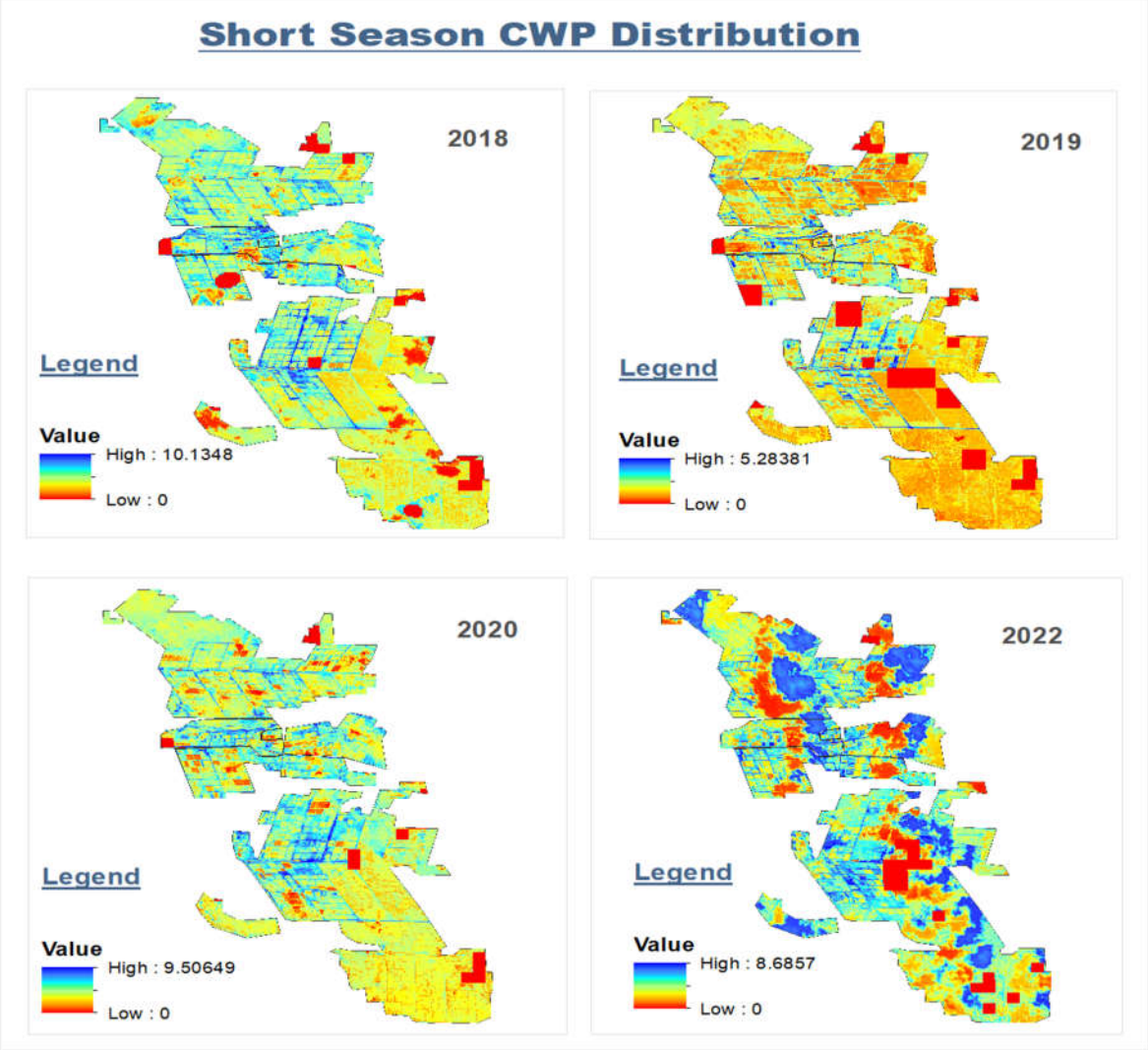

Figure 4.8: 2018 to 2022 short season CWP estimates maps

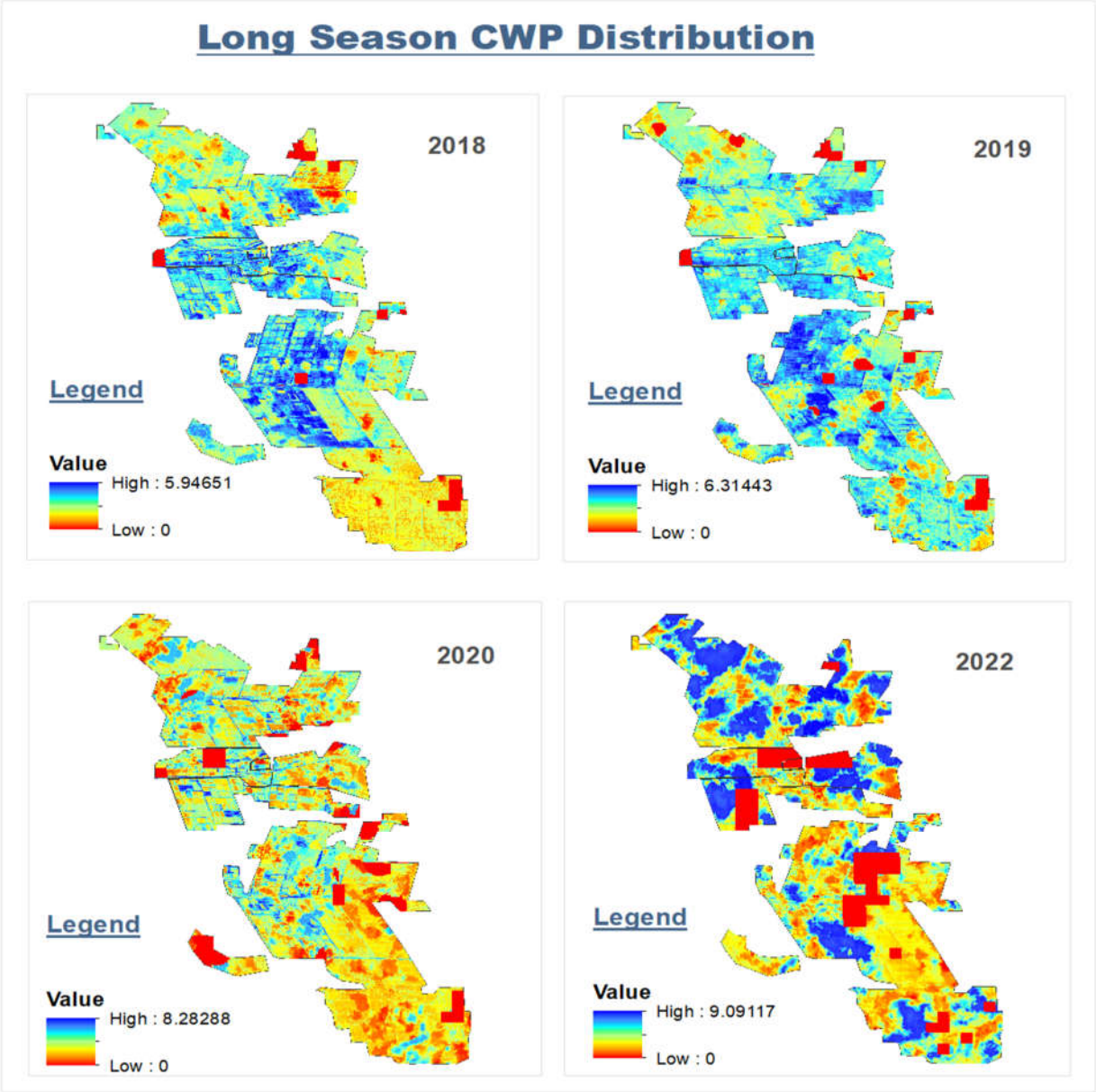

Figure 4.9: 2018 to 2022 long season CWP

4.5 CWP, Yield and ET Trend View

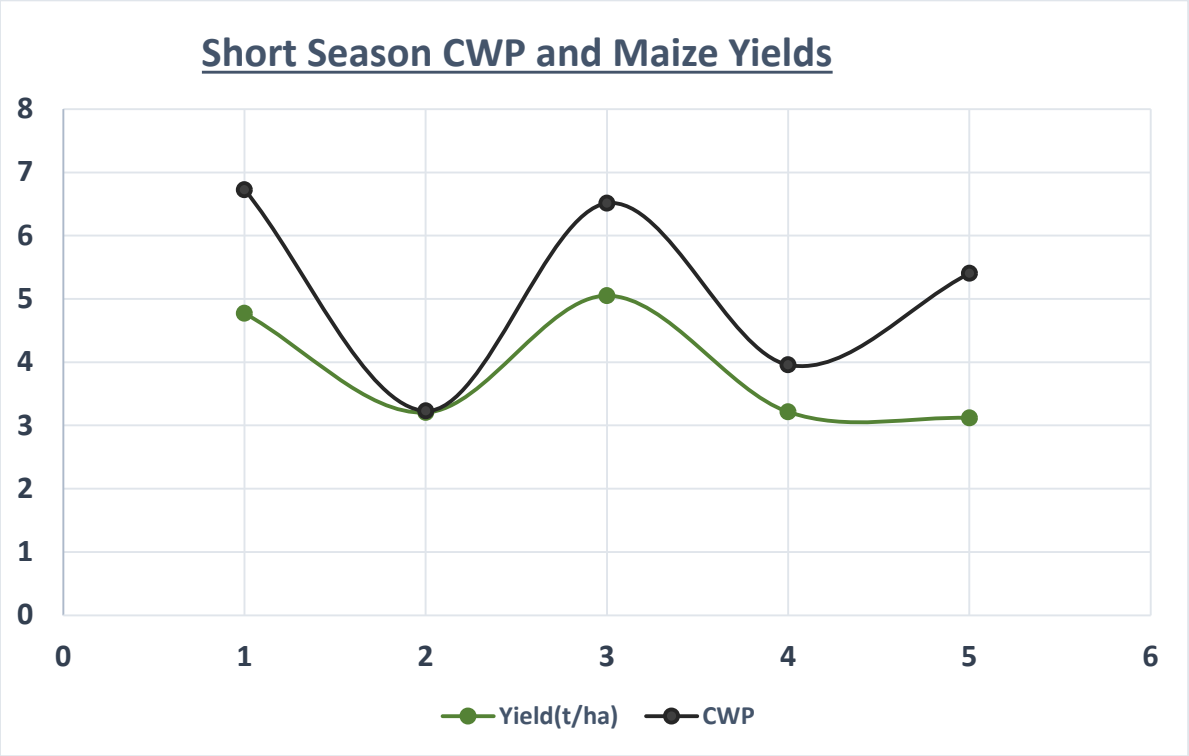

Figure 4.10: Yearly Yield compared with CWP

In addition to the spatial maps, zonal statistics were calculated for each season and year to quantify crop water productivity shown (Table 4.2). The reference evapotranspiration (ET0), actual evapotranspiration (ETa), ETa standard deviation, yield, and CWP were summarized. This provides the temporal variability in key water use and productivity metrics.

CWP showed differences between the short and long growing seasons. In the short season, CWP ranged from 3.23 kg/m3 in 2019 up to 6.73 kg/m3 in 2018. For the long season, CWP was lower, varying between 4.21 kg/m3 in 2018 to 5.88 kg/m3 in 2022. Yield also fluctuated year-to-year, with lowest values in 2019 short season (3.21 t/ha) and 2021 long season (3.34 t/ha).

To further analyze the relationships between water use, yield, and CWP, line graphs and bar plots were created. Figure 4.10 shows the connected trends in CWP and yield over time for both seasons. CWP and yields decreased in 2019 and 2021 short seasons compared to 2018, while remaining more stable in the long season.

Meanwhile, Figures 4.11a and 4.11b illustrate the comparative bars of CWP, yield, and ETa standard deviation by season. The highest CWP and yields aligned with lower ETa variability in 2018 short season and 2022 long season. ETa deviation was larger in years with reduced productivity.

Overall, the temporal graphs coupled with the spatial CWP maps provide insights into the factors influencing crop water productivity over the study period. The statistics and visualizations can guide water and yield optimization.

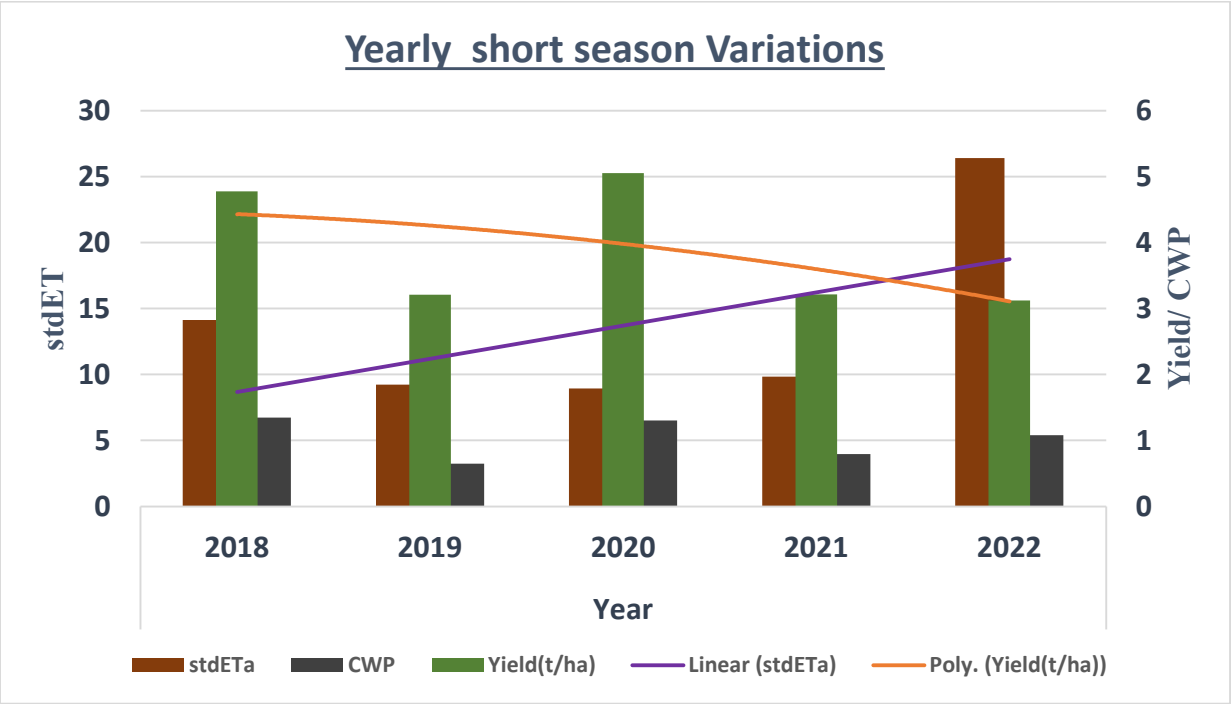

Figure 4.11a: CWP, Yield, and standard ET yearly short season trend

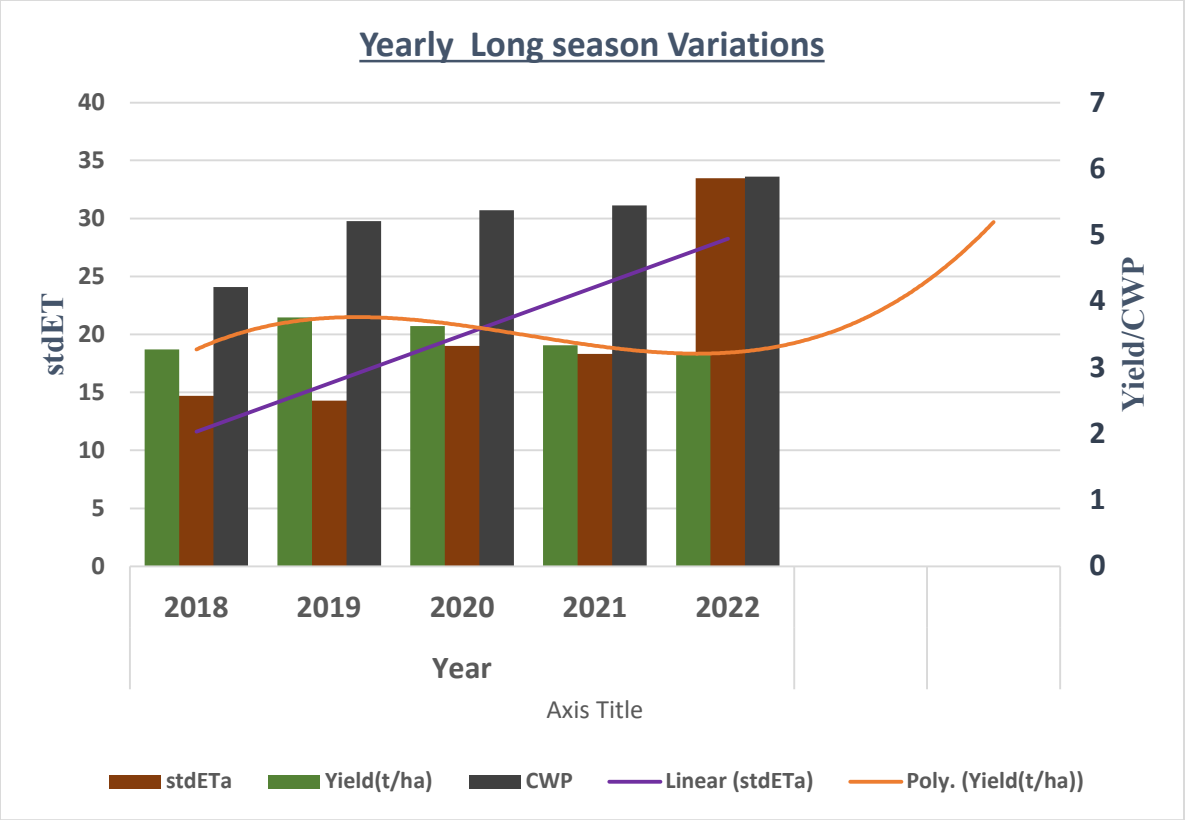

Figure 4.11b: CWP, Yield, and standard ET yearly long season trend

Short Season Statistics						
		ET0	Eta	stdETa	Yield(t/ha)	CWP
Year	2018	237.0842	69.47594	14.12928	4.776366357	6.730136
	2019	258.0159	96.215	9.227823	3.207342922	3.233628
	2020	237.2859	76.05709	8.942988	5.052628943	6.515204
	2021	261.6644	79.7649	9.837985	3.215566055	3.960766
	2022	249.1607	58.34623	26.39416	3.121359342	5.406843

Long Season Statistics						
		ET0	Eta	stdETa	Yield(t/ha)	CWP
Year	2018	215.4942	75.8447	14.69787	3.271972696	4.213657
	2019	227.6036	72.08	14.28246	3.7555	5.21018
	2020	243.2024	67.29996	19.00252	3.626553298	5.372413
	2021	249.0766	61.38575	18.32356	3.336088949	5.443546
	2022	252.2586	57.67675	33.46675	3.222519736	5.881332

Table 4.2: Regional Statistics

4.6 Relative Importance of CWP estimation parameters

A correlation matrix was generated to examine the relationships between the vegetation indices, remote sensing metrics, and the target variables of crop water productivity (CWP), evapotranspiration (ET), and yield whose results is as in figure 4.12 below.

The vegetation indices of EVI, GNDVI, and SAVI showed strong positive correlations with each other, with coefficients ranging from 0.83 to 1.0. These three indices also demonstrated positive correlations with the target variables, with GNDVI having the strongest correlations of 0.19 with yield, 0.07 with CWP, and 0.05 with ET.

The remote sensing metrics of SR, EDI, TCI, and albedo had strong inter-correlations, with coefficients from 0.48 to 0.79. Of these, EDI and TCI showed the highest correlations with yield at 0.27 and 0.29, respectively. Albedo and land surface temperature (LST) were most strongly correlated with CWP, at -0.64 and -0.49.

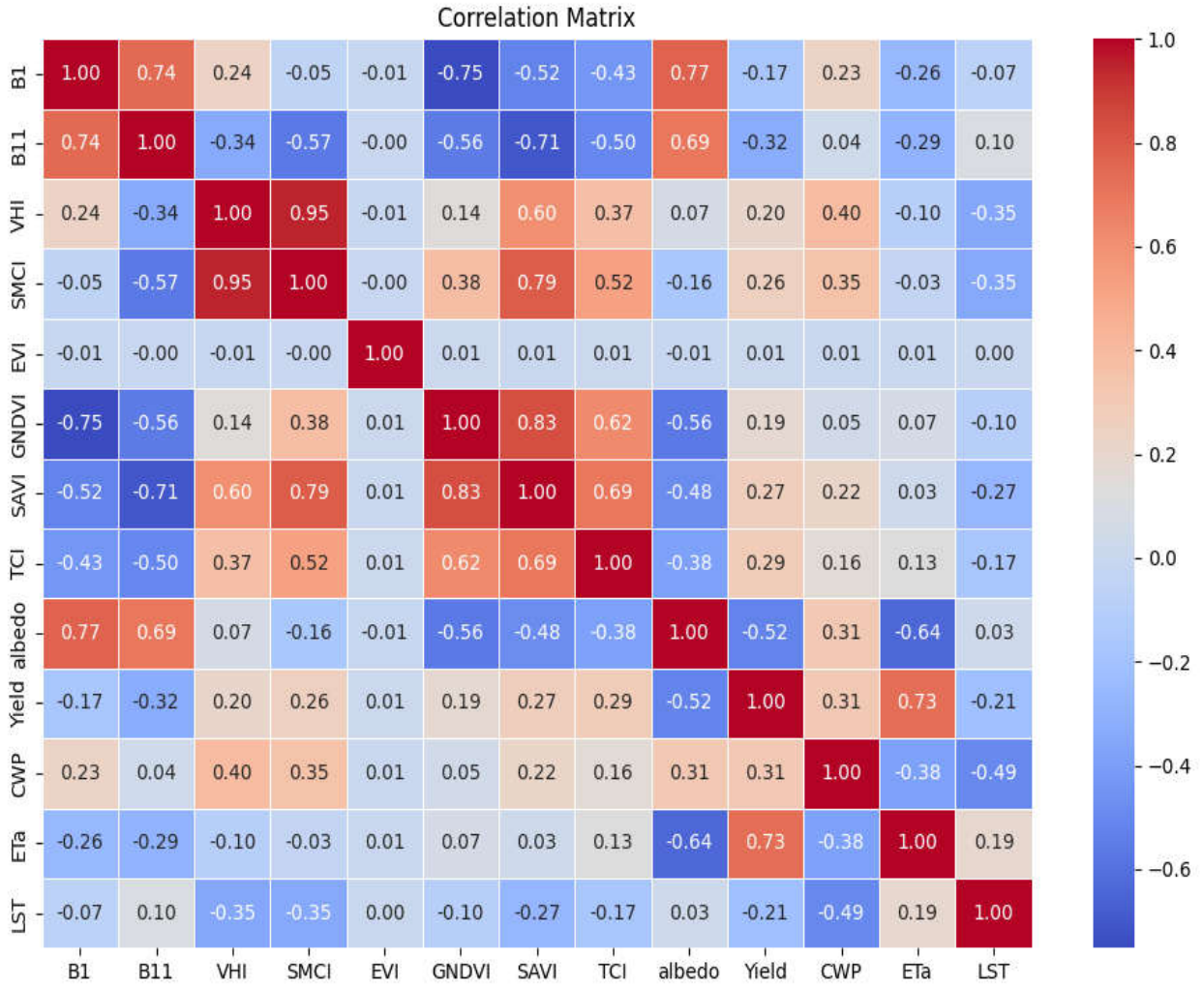

Figure 4.12: Machine learning Variables Correlation matrix

An XGBoost model was developed to predict crop water productivity (CWP), yield, and actual evapotranspiration (ETa). The model's performance was evaluated using the metrics of mean absolute error (MAE), R-squared (R2), root mean squared error (RMSE), and mean squared error (MSE).

For CWP, the model achieved an R2 of 0.79, indicating the model explains 79% of the variability in the true CWP values. The RMSE and MSE were 0.58 and 0.34, respectively, showing the errors made in predicting CWP. The model performed very well for yield prediction, with an R2 of 0.88 and low RMSE of 0.45 and MSE of 0.20. This demonstrates the model's strong ability to predict crop yield. For ETa, the model had an R2 of 0.91, so over 90% of the ETa variation is explained. However, the errors were higher compared to CWP and yield, with RMSE of 7.27 and

MSE of 52.87. So, the model's predictions of ETa, while still good, were less accurate than for the other targets.

Overall, the XGBoost model showed strong performance for predicting CWP, yield, and ETa from the given data. The highest accuracy was achieved for yield, followed by ETa and CWP. These evaluation metrics quantify the model's ability to generalize and accurately estimate the target variables for this crop system.

The trained XGBoost model was used to generate predictions for crop water productivity (CWP), yield, and actual evapotranspiration (ETa) across the Bura Irrigation Scheme. Statistical summaries were calculated on the predictions and compared to the summaries of the actual field data. The model predictions had a mean of 6.12, close to the actual mean of 5.85 for CWP. The standard deviation of the predictions was 0.92 compared to 0.88 for the real data.

The predicted yield had a mean of 3.14 and standard deviation of 1.55. The actual yield statistics were a mean of 3.10 and standard deviation of 1.41. So, the yield predictions aligned well with the real yield distribution. ETa prediction on the other hand showed the largest difference from the field data. The predicted ETa mean was 56.29 and standard deviation was 32.92. However, the actual ETa mean was 56.92 with a standard deviation of 29.99. So, the model overestimated the ETa mean slightly.

The scatter plot in Figure 4.13 allows visualization of the relationship between the model's predicted values and actual field measured values for crop water productivity (CWP), yield, and actual evapotranspiration (ETa). Each point on the plot represents one pair of a predicted and observed value. The distribution and clustering of these points provides insight into how well the predictions correspond to the real data.

A linear fit line is added to the scatter plot, with an equation of $y=0.98x + 0.41$. The slope of 0.98 indicates a nearly 1:1 agreement between predicted and actual values across the variables. This slope close to 1 demonstrates the strong correlation between model predictions and ground truth data. The intercept of 0.41 suggests a small bias where the model is slightly overestimating the field values. Overall, the fit line quantifies the close linear relationship between predictions and measurements.

4.7 Xgboost Model results

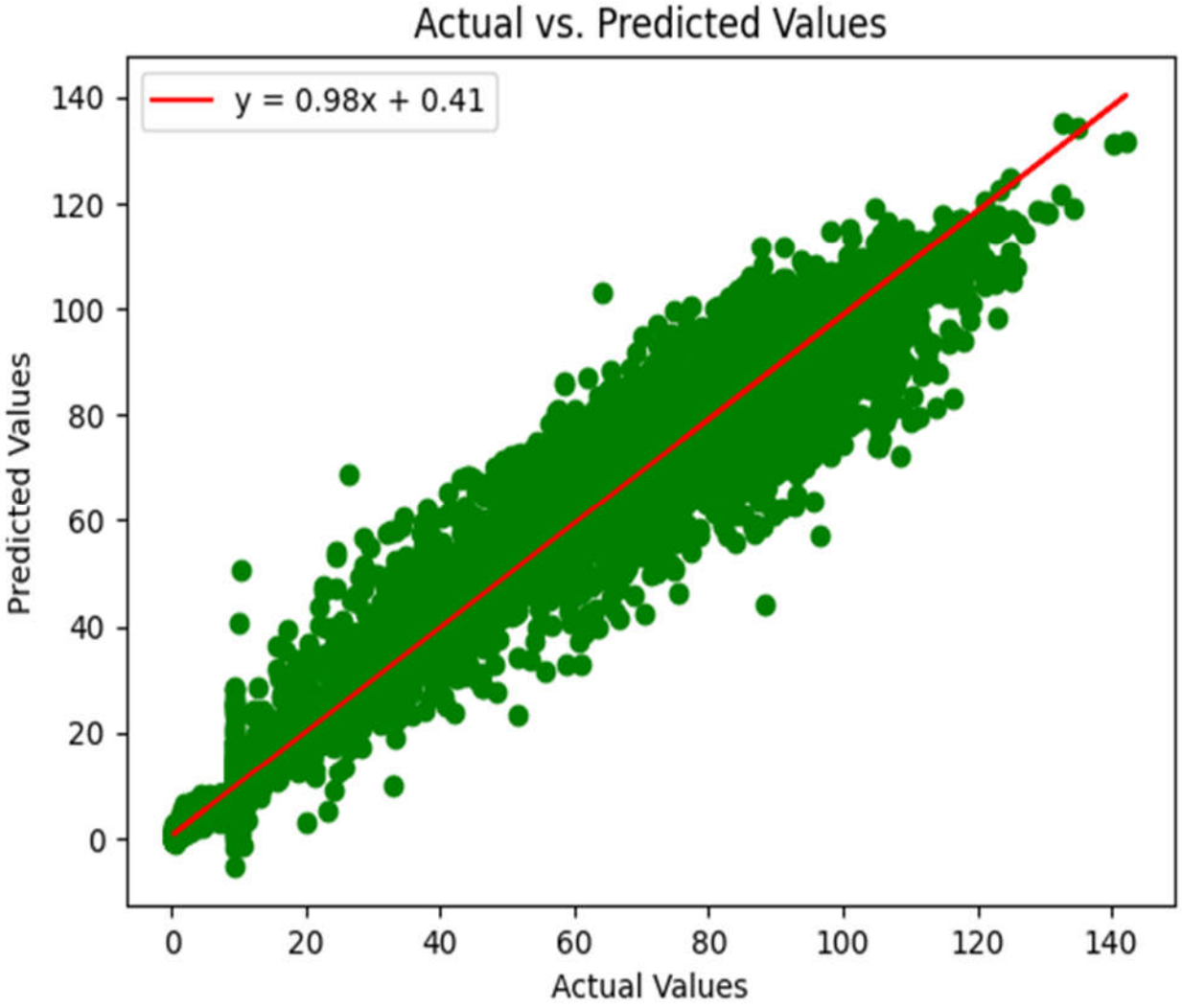

Figure 4.13: XGBoost CWP, yield and Eta Scatter plot.

4.8 Validity of Machine Learning Model (XGBoost)

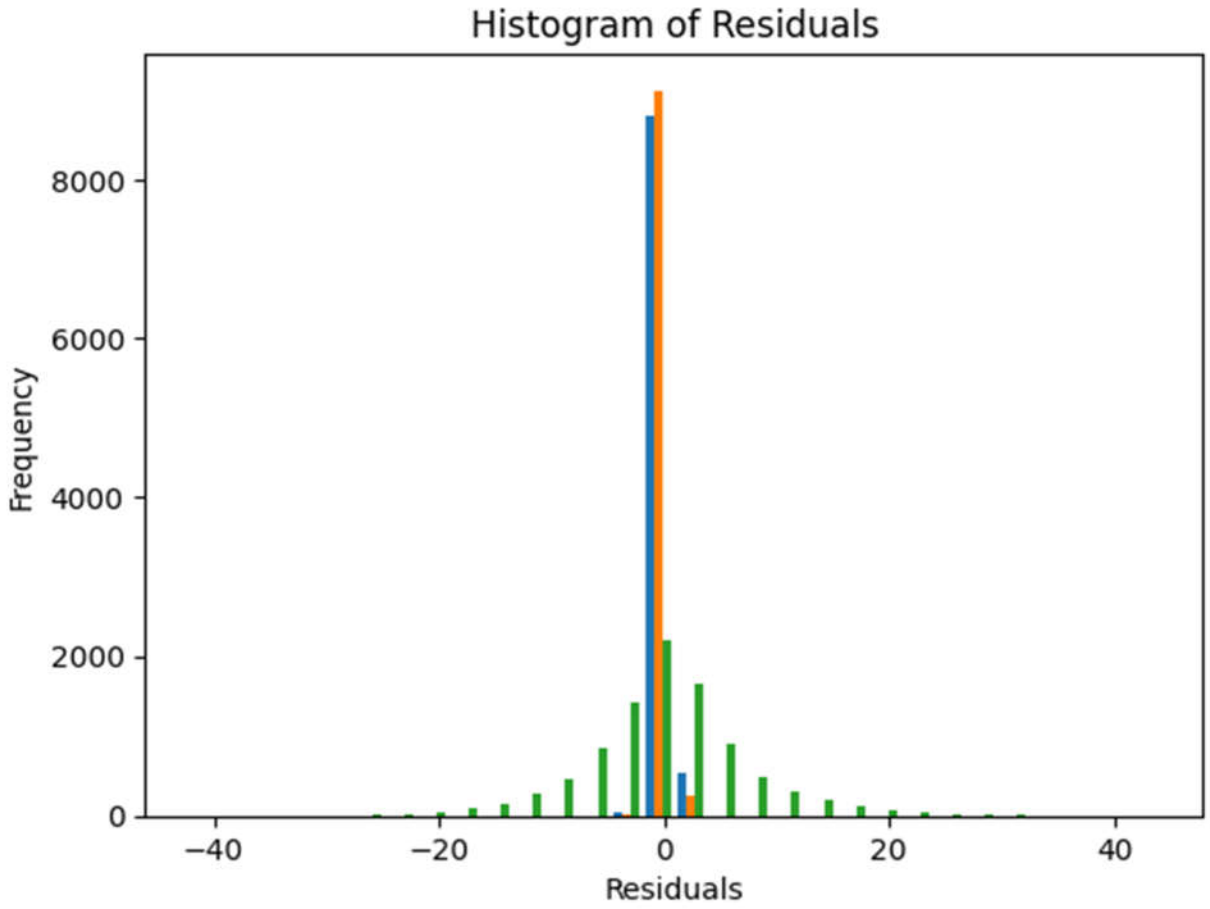

Figure 4.14: XGBoost model prediction residuals.

A residual plot (figure 4.14) was generated to evaluate the trained XGBoost model by plotting a histogram of the prediction residuals (errors). The residual is the difference between the model's predicted value and the actual observed value for each data point. The residual plot shows the highest frequency of residuals near 0, with decreasing frequencies towards the left and right extremes. The concentration of residuals near 0 indicates the model is making smaller errors overall, predicting values close to the actual observations. The tapering residuals further from 0 suggest larger prediction errors occur less often. The symmetrical, bell-curve-like shape shows the errors are approximately normally distributed, which is ideal.

No strong skewness or multiple peaks are apparent, signifying the lack of systemic biases in the model's errors. The residual plot demonstrates this XGBoost

model is accurately predicting the target variables, with the majority of errors small and centered on 0. Therefore, the residual distribution validates the model's strong performance and ability to generalize predictions across the dataset with minimal bias.

The trained XGBoost model was then directly applied to a 2022 satellite image (daily collection for the specified short and long maize growing season) covering the Bura Irrigation Scheme area. Predictions were generated for crop water productivity (CWP), yield, and actual evapotranspiration (ETa) across the scheme by utilizing various spectral bands and vegetation indices as model inputs.

The zonal statistics of the predicted CWP had a mean of 5.80 and standard deviation of 0.25 across the study area. Compared to the actual field-measured CWP statistics of a mean of 5.85 and standard deviation of 0.88, the predicted mean is very close to the true value. However, the model underestimates the variability in CWP, as seen in the lower standard deviation. For predicted yield, the model estimated a mean of 3.27 and standard deviation of 0.50. The actual yield measurements had a mean of 3.10 and higher standard deviation of 1.41. So, the model overestimates the true yield mean slightly but underestimates the yield variability across the scheme.

The largest difference between predicted and measured statistics is seen for ETa. The model predicted an ETa mean of 59.25 with a standard deviation of 12.78. But the ground measurements showed a lower ETa mean of 56.92 and much higher variability of 29.99. This indicates the model is overestimating ETa while also underestimating the spatial differences in ETa across the study region.

5. Discussion

5.1 Crop Phenology Dynamics

Analysis of vegetation indices over time provided insights into crop growth stages and phenology patterns in the Bura Irrigation Scheme. The NDVI and EVI curves showed two distinct maize growing periods aligned with the short and long rainy seasons.

Sowing typically occurred around late January and in the short season sowing is done in late August to early September. Peak greenness and canopy cover was reached at tasseling or silking around late April-May in the long season and in the short season around late September-October. Finally, maturity and senescence phases occurred around late July to early August for long season maize and mid-December for short season crops.

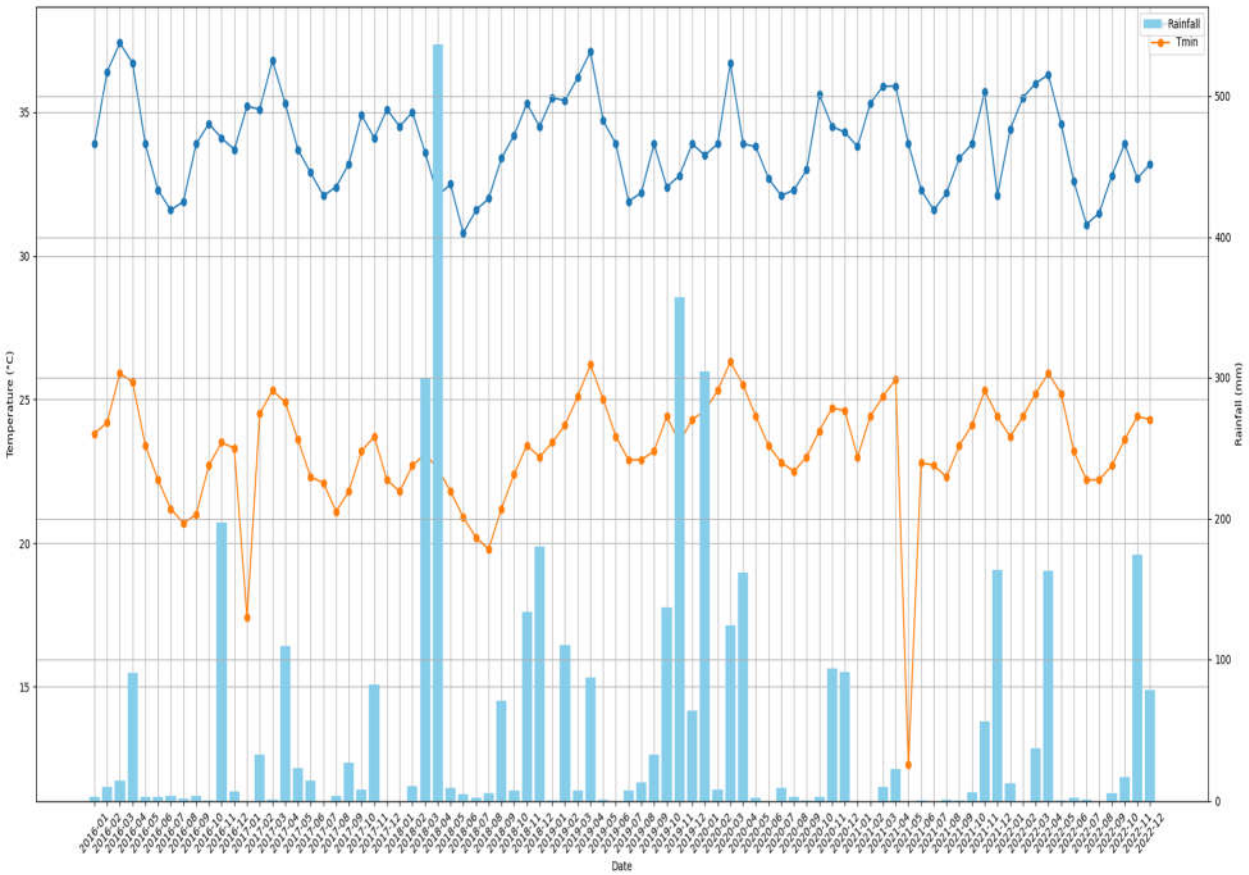

Figure 5.1: Local Seasonal Temperature and rainfall variability

These patterns agree well with crop calendars for the region reported by KMD and local agricultural agencies (Mugai et al., 2019; KALRO, 2022). Figure 5.1 shows the actual local weather pattern based on KMD dataset.

The bimodal cycles enable year-round production but can complicate irrigation and other management. In particular, the short season growth stage is vulnerable to terminal moisture stress due to cessation of rains (KMD, 2022).

Phenology monitoring showed that sowing periods were less discrete than typical rainfed systems, likely due to year-round irrigation availability allowing continuous cropping. Overlaps in sowing and maturity phases indicate farmers' capacity to stagger planting dates to manage water demand and respond to climate variability.

Capturing crop growth dynamics is critical for indexing vegetation health as well as parameterizing CWP models. For example, relating ETa patterns to different crop stages helps diagnose likely causes of water stress (e.g., emergence vs. grain filling). Similarly, timing of NDVI peaks and yield estimation is keyed to specific developmental milestones like flowering and maturity (Bastiaanssen & Ali, 2003).

5.2 Analysis of Yield and ET results

The light use efficiency modeling approach enabled mapping of maize yield across the study area. Estimated yields showed high spatio-temporal variability, ranging from 429 kg/ha to 9178 kg/ha as evidenced in the results. Research has found that factors like soil fertility, crop genetics, and management practices can significantly influence productivity in this region (Muli et al., 2015). While the model provides useful yield estimations, ground-truthing and calibration using field measurements could help refine parameterization and improve accuracy over time (Bastiaanssen & Ali, 2003). Field collection of yield data through surveys or on-farm trials supports continued advancement of the remote sensing-based yield model.

Evapotranspiration (ET) was estimated using the SEBAL energy balance model, incorporating both satellite imagery and weather data. Estimated ET fluctuated between 42.7 mm and 117 mm over the study period, reflecting changing crop water demand. Prior research found that maize ET in similar environments varies depending on climate, soils, and irrigation. Tracking

ET provides insights into crop water usage dynamics and factors influencing productivity like water stress (Allen et al., 1998). However, uncertainties remain in the ET modeling, requiring further validation using lysimetry or other field techniques. Improved characterization of soil hydraulic properties, crop development, and micrometeorology can aid ET estimation.

5.3 Spatio-temporal Patterns in Crop Water Productivity

The crop water productivity (CWP) analysis for the Bura Irrigation Scheme revealed distinct spatial and temporal patterns. CWP showed high variability both between seasons and across years. In the short growing season, CWP was lowest in 2019 at 3.23 kg/m3 and highest in 2018 at 6.73 kg/m3. For the long season, CWP ranged from` 4.21 kg/m3 in 2018 to 5.88 kg/m3 in 2022. This aligns with findings by Muigai et al. (2019) who reported CWP between 3.9-6.5 kg/m3 for maize in the Bura scheme depending on planting date.

This variability highlights the impacts of changing weather patterns, differences in cropping systems, and water management across the scheme (Blatchford et al., 2018). Years with higher CWP like 2018 short season suggest better moisture availability, while low CWP in 2019 short growing period indicates water limitation reduced productivity despite irrigation potential (Sarshad et al., 2021). As CWP integrates crop yield and actual evapotranspiration, it provides an index of plant growth, vigor, and the efficiency of water use (Hellegers et al., 2009; Booker & Trees, 2020).

The temporal CWP fluctuations demonstrate the need for flexible, responsive water management to account for inter-annual weather variability and associated crop water requirements in this semi-arid region (Hommadi & Almasraf, 2019). For instance, the higher CWP in 2018 short season resulted from sufficient moisture availability to meet crop demands. But in 2019, CWP declined as crops faced water limitation during the critical growth stages, reducing yields (Talpur et al., 2023). Adapting irrigation scheduling and volume based on real-time monitoring of crop water use and plant water stress could stabilize productivity over variable seasons.

CWP responds to agronomic practices like irrigation method, planting density, and fertilizer application. Thus, the CWP assessment provides an integrated measure of crop

performance and water use efficiency to guide management. Monitoring of CWP using remote sensing offers a scalable approach to benchmarking and improving agricultural water productivity in the area. However, several sources of uncertainty persist and require ongoing research. Soil variability, microclimate fluctuations, and complex crop-water interactions may not be fully captured (Gibson et al., 2018). Field instrumentation like soil moisture probes, weather stations, and plant water status sensors can provide data to refine parameterization and improve estimation performance (Dalla Marta et al., 2018). Higher resolution inputs from satellite, drone or airplane remote sensing could better resolve within-field heterogeneity.

5.4 Machine Learning for Enhanced CWP Estimation

Machine learning techniques have emerged as powerful tools for enhancing crop water productivity (CWP) estimation using remote sensing and meteorological data. As demonstrated in this study, models like XGBoost can effectively integrate and analyze different data sources to generate reliable predictions of key parameters including CWP, yield, and evapotranspiration (Elbeltagi et al., 2022).

The implementation of XGBoost allowed the exploitation of complex interactions and patterns within the dataset that would be difficult to model using traditional statistical approaches. As discussed by Virnodkar et al. (2020), machine learning algorithms like XGBoost have distinct advantages for handling large, multi-dimensional agricultural datasets comprising various soil, climate, spectral and crop-specific variables. By capturing non-linear relationships, high-order interactions, and latent data structures, the XGBoost model provided robust generalization capability beyond the training data.

The model evaluation confirmed the strong predictive performance of XGBoost for the target output variables. Metrics like the coefficient of determination (R2) and residual analysis demonstrated good model fit with minimal bias. As noted by Patel et al. (2021), machine learning approaches require careful validation to assess real-world applicability. The residual errors centered around zero provided evidence that XGBoost could produce reliable CWP, yield and ET estimates from unseen data in the operational setting.

An additional benefit of using XGBoost was the intrinsic feature selection, ranking the most informative input variables through each iteration of tree splits during model training (Islam et al., 2023). This allowed automated optimization of the many spectral, soil, vegetation and climate variables available to determine an optimal subset for accurate CWP and ET prediction. Such data-driven variable selection removes subjective biases common in manual techniques.

Overall, the machine learning methods implemented significantly advanced the crop water productivity assessment, providing a scalable approach to integrating large datasets and extracting actionable insights.

6. Conclusions

In conclusion, this research aimed to estimate crop water productivity (CWP) for maize in the Bura Irrigation Scheme from 2018-2022 using remote sensing and machine learning techniques. The goal was to support improved water management and agricultural resilience in this semi-arid region prone to drought and water scarcity.

The study incorporated satellite imagery across multiple sensors (Landsat, Sentinel-2, MODIS) as well as meteorological data from ERA5 and local weather stations. Vegetation indices including NDVI and EVI enabled crop growth stage monitoring while ET was modelled using SEBAL energy balance and the FAO Penman-Monteith method. Crop yield was estimated using a light use efficiency approach relating biomass production to absorbed photosynthetically active radiation and harvest index.

The generated CWP maps and statistics revealed distinct spatial patterns, with higher productivity aligning to intensely irrigated zones while southern areas showed poorer CWP. Temporal fluctuations occurred between seasons and years, highlighting the impacts of variable weather and water availability on crop-water dynamics. Estimated CWP ranged from 3.2-6.7 kg/m3 over the period, agreeing with previous local studies. The yield model performed well but could be further improved through calibration with field measurements.

Machine learning, specifically the XGBoost algorithm, was implemented to enhance CWP, yield and ET estimation by exploiting complex data relationships. The model evaluation confirmed excellent predictive capability based on metrics like R2, RMSE and residual analysis. Applied to unseen satellite imagery, the trained model generated reasonable CWP, yield and ET estimates across the scheme.

Finally, this study highlighted the capabilities of emerging digital techniques for water productivity monitoring to support agricultural sustainability. With further refinement, the developed methods could aid real-time irrigation decisions and benchmarking to improve yields, optimize water utilization and build climate change resilience across the region. Integrating such data-driven approaches with water governance and policy frameworks will be essential to translate information into action for sustainable agricultural water management.

Recommendations

Expand the ground data collection to additional locations within the irrigation scheme. While the current analysis relied primarily on remotely sensed data, gridded, and single station local weather datasets, collecting in situ data on crop yields, soil moisture, weather parameters, and water use at more sites would allow for improved validation and parameterization of the CWP model across the spatial extent of the scheme. This could be achieved through test plots and intensive measurement campaigns during critical crop growth stages.

Incorporate higher-resolution satellite imagery from sensors such as GeoEye, Pleiades, or drone and airborne data. The 10-30 m resolution data used currently limits characterization of fine-scale heterogeneity in factors driving field-level variations in CWP. Sub-meter satellites could better capture soil, topographic and drainage variability to diagnose tightly localized yield constraints.

Test alternate deep learning algorithms and ensemble approaches to improve generalizability. While XGBoost performed well presently, evaluating other techniques like neural networks or combinations of statistical and deep learning models may lead to better out-of-sample prediction accuracy. Tuning model structural complexity could prevent overfitting given the limited training dataset size. Augmenting input data through generative adversarial networks (GANs) is another avenue to explore.

Integrate findings into a user-friendly decision support system for local stakeholders. To enable accessible adoption of the CWP insights by irrigation scheme managers and agricultural extension officers, packaging the results into an interactive web dashboard or mobile application is imperative. The system could provide real-time visualization of the spatial CWP and yield patterns while summarizing trends and variability for the region. User input mechanisms to customize recommendations based on crop types, field locations and available budget should also be enabled for practical utility. Leveraging such ICT tools can bridge the research-implementation gap more effectively.

7. References

Geng, L., Che, T., Ma, M., Tan, J., & Wang, H. (2021). Corn biomass estimation by integrating remote sensing and long-term observation data based on machine learning techniques. *Remote Sensing*, *13*(12), 2352. https://doi.org/10.3390/rs13122352

Mountrakis, G., Im, J., & Ogole, C. (2011). Support Vector Machines in remote sensing: A Review. *ISPRS Journal of Photogrammetry and Remote Sensing*, *66*(3), 247–259. https://doi.org/10.1016/j.isprsjprs.2010.11.001

Xu, L., Yu, H., Chen, Z., Du, W., Chen, N., & Huang, M. (2023). Hybrid deep learning and S2S model for improved sub-seasonal surface and root-zone soil moisture forecasting. *Remote Sensing*, *15*(13), 3410. https://doi.org/10.3390/rs15133410

Pedregosa, F., Varoquaux, G., Gramfort, A., Michel, V., Thirion, B., Grisel, O., Blondel, M.,Prettenhofer, P., Weiss, R., Dubourg, V., Vanderplas, J., Passos, A., Cournapeau, D., Brucher, M., Perrot, M., & Duchesnay, E. (2011). Scikit-learn: Machine Learning in Python. Journal of Machine Learning Research, 12, 2825–2830.

Cemek, B., Tasan, S., Canturk, A., Tasan, M., & Simsek, H. (2023). Machine learning techniques in estimation of eggplant crop evapotranspiration. *Applied Water Science*, *13*(6). https://doi.org/10.1007/s13201-023-01942-1

Gebremedhin, M. A., Lubczynski, M. W., Maathuis, B. H. P., & Teka, D. (2022). Deriving potential evapotranspiration from satellite-based reference evapotranspiration, Upper Tekeze Basin, northern Ethiopia. *Journal of Hydrology: Regional Studies*, *41*, 101059. https://doi.org/10.1016/j.ejrh.2022.101059

Wang, Q.-Q., Geng, C.-X., Wang, L., Zheng, T.-T., Jiang, Q.-H., Yang, T., Liu, Y.-Q., & Wang, Z. (2023). Water conservation and ecological water requirement prediction of mining area in arid region based on RS-GIS and invest: A case study of bayan obo mine in Baotou, China. *Sustainability*, *15*(5), 4238. https://doi.org/10.3390/su15054238

Laipelt, L., Henrique Bloedow Kayser, R., Santos Fleischmann, A., Ruhoff, A., Bastiaanssen, W., Erickson, T. A., & Melton, F. (2021). Long-term monitoring of

evapotranspiration using the SEBAL algorithm and Google Earth Engine Cloud Computing. *ISPRS Journal of Photogrammetry and Remote Sensing*, *178*, 81–96. https://doi.org/10.1016/j.isprsjprs.2021.05.018

Jaafar, H. H., & Ahmad, F. A. (2020). Time series trends of landsat-based ET using automated calibration in metric and SEBAL: The Bekaa Valley, Lebanon. *Remote Sensing of Environment*, *238*, 111034. https://doi.org/10.1016/j.rse.2018.12.033

Tasumi, M., Allen, R. G., & Trezza, R. (2008). At-surface reflectance and albedo from satellite for operational calculation of Land Surface Energy Balance. *Journal of Hydrologic Engineering*, *13*(2), 51–63. https://doi.org/10.1061/(asce)1084-0699(2008)13:2(51)

Gonçalves, I. Z., Ruhoff, A., Laipelt, L., Bispo, R. C., Hernandez, F. B. T., Neale, C. M. U., Teixeira, A. H. C., & Marin, F. R. (2022). Remote Sensing-based evapotranspiration modeling using geesebal for sugarcane irrigation management in Brazil. *Agricultural Water Management*, *274*, 107965. https://doi.org/10.1016/j.agwat.2022.107965

Huang, L. *et al.* (2022) 'A two-stage light-use efficiency model for improving gross primary production estimation in Agroecosystems', *Environmental Research Letters*, 17(10), p. 104021. https://doi.org/10.1088/1748-9326/ac8b98

Bastiaanssen, W.G.M. and Ali, S. (2003) 'A new crop yield forecasting model based on satellite measurements applied across the Indus Basin, Pakistan', *Agriculture, Ecosystems & Environment*, 94(3), pp. 321–340. https://doi.org/10.1016/s0167-8809(02)00034-8.

Moriondo, M., Maselli, F. and Bindi, M. (2007) 'A simple model of regional wheat yield based on NDVI data', *European Journal of Agronomy*, 26(3), pp. 266–274. https://doi.org/10.1016/j.eja.2006.10.007 .

Dhau, I., Dube, T., & Mushore, T. D. (2019). Examining the prospects of sentinel-2 multispectral data in detecting and mapping maize streak virus severity in smallholder Ofcolaco farms, South Africa. *Geocarto International*, *36*(16), 1873–1883. https://doi.org/10.1080/10106049.2019.1669724

Laonamsai, J., Julphunthong, P., Saprathet, T., Kimmany, B., Ganchanasuragit, T., Chomcheawchan, P., & Tomun, N. (2023). Utilizing NDWI, MNDWI, Savi, WRI, and Awei for estimating erosion and deposition in Ping River in Thailand. *Hydrology*, *10*(3), 70. https://doi.org/10.3390/hydrology10030070

Bolfe, É. L., Parreiras, T. C., Silva, L. A., Sano, E. E., Bettiol, G. M., Victoria, D. de, Sanches, I. D., & Vicente, L. E. (2023). Mapping agricultural intensification in the Brazilian savanna: A machine learning approach using harmonized data from Landsat Sentinel-2. *ISPRS International Journal of Geo-Information*, *12*(7), 263. https://doi.org/10.3390/ijgi12070263

Agilandeeswari, L., Prabukumar, M., Radhesyam, V., Phaneendra, K. L., & Farhan, A. (2022). Crop classification for agricultural applications in hyperspectral remote sensing images. *Applied Sciences*, *12*(3), 1670. https://doi.org/10.3390/app12031670

Khan, M. I., Liu, D., Fu, Q., & Faiz, M. A. (2017). Detecting the persistence of drying trends under changing climate conditions using four meteorological drought indices. *Meteorological Applications*, *25*(2), 184–194. https://doi.org/10.1002/met.1680

Sánchez, N., González-Zamora, Á., Piles, M., & Martínez-Fernández, J. (2016). A new soil moisture agricultural drought index (SMADI) integrating Modis and smos products: A case of study over the Iberian Peninsula. *Remote Sensing*, *8*(4), 287. https://doi.org/10.3390/rs8040287

Zhao, Y., Zhang, J., Bai, Y., Zhang, S., Yang, S., Henchiri, M., Seka, A. M., & Nanzad, L. (2022). Drought monitoring and performance evaluation based on machine learning fusion of multi-source remote sensing drought factors. *Remote Sensing*, *14*(24), 6398. https://doi.org/10.3390/rs14246398

Gao, F., Hilker, T., Zhu, X., Anderson, M., Masek, J., Wang, P., & Yang, Y. (2015). Fusing Landsat and Modis data for vegetation monitoring. *IEEE Geoscience and Remote Sensing Magazine*, *3*(3), 47–60. https://doi.org/10.1109/mgrs.2015.2434351

Wu, M., Huang, W., Niu, Z., Wang, C., Li, W., & Yu, B. (2018). Validation of Synthetic Daily Landsat NDVI time series data generated by the improved spatial and temporal data fusion approach. *Information Fusion*, *40*, 34–44. https://doi.org/10.1016/j.inffus.2017.06.005

Luo, Y., Guan, K., Peng, J., Wang, S., & Huang, Y. (2020). Stair 2.0: A generic and automatic algorithm to Fuse Modis, landsat, and sentinel-2 to generate 10 m, daily, and cloud-/gap-free surface reflectance product. *Remote Sensing*, *12*(19), 3209. https://doi.org/10.3390/rs12193209

Dhillon, M. S., Kübert-Flock, C., Dahms, T., Rummler, T., Arnault, J., Steffan-Dewenter, I., & Ullmann, T. (2023). Evaluation of modis, Landsat 8 and sentinel-2 data for accurate crop yield predictions: A case study using STARFM NDVI in Bavaria, Germany. *Remote Sensing*, *15*(7), 1830. https://doi.org/10.3390/rs15071830

Pelosi, A., Belfiore, O. R., D'Urso, G., & Chirico, G. B. (2022). Assessing crop water requirement and y9ield by combining ERA5-land reanalysis data with CM-SAF satellite-based Radiation Data and sentinel-2 satellite imagery. *Remote Sensing*, *14*(24), 6233. https://doi.org/10.3390/rs14246233

Copernicus, E. (2018, June 14). *Copernicus Climate Data Store*. Copernicus Climate Data Store |. https://cds.climate.copernicus.eu/cdsapp#!/dataset/reanalysis-era5-single-levels?tab=overview.

Thapa, B., Lovell, S., & Wilson, J. (2023). Remote Sensing and machine learning applications for aboveground biomass estimation in agroforestry systems: A Review. *Agroforestry Systems*, *97*(6), 1097–1111. https://doi.org/10.1007/s10457-023-00850-2

Emami, M., Ahmadi, A., Daccache, A., Nazif, S., Mousavi, S.-F., & Karami, H. (2022). County-level irrigation water demand estimation using Machine Learning: Case Study of California. *Water*, *14*(12), 1937. https://doi.org/10.3390/w14121937

Ashwitha, A., & Latha, C. A. (2022). Crop recommendation and yield estimation using machine learning. *Journal of Mobile Multimedia*. https://doi.org/10.13052/jmm1550-4646.18320

Holzman, M. E., & Rivas, R. E. (2016). Early maize yield forecasting from remotely sensed temperature/vegetation index measurements. *IEEE Journal of Selected Topics in Applied Earth Observations and Remote Sensing*, *9*(1), 507–519. https://doi.org/10.1109/jstars.2015.2504262

Wang, Z., Shu, Y., Zhang, S., Li, H., & Lei, Y. (2009). Evaluating crop land productivity using modis derived time serious field greenness and water index in North China Plain. *SPIE Proceedings*. https://doi.org/10.1117/12.830775

Singh, P., Singh, A., & Kumar Upadhyay, R. (2021). A web based Google Earth engine approach for irrigation scheduling in Uttar Pradesh India using Crop Water Stress Index. *American Journal of Remote Sensing*, *9*(1), 42. https://doi.org/10.11648/j.ajrs.20210901.15

Tang, X., Li, H., Griffis, T., Xu, X., Ding, Z., & Liu, G. (2015). Tracking ecosystem water use efficiency of cropland by exclusive use of Modis Evi Data. *Remote Sensing*, *7*(9), 11016–11035. https://doi.org/10.3390/rs70911016

Jaafar, H. H., & Ahmad, F. A. (2015). Crop yield prediction from remotely sensed vegetation indices and primary productivity in arid and semi-arid lands. *International Journal of Remote Sensing*, *36*(18), 4570–4589. https://doi.org/10.1080/01431161.2015.1084434

Farrell, M., Gili, A., & Noellemeyer, E. (2018). Spectral indices from aerial images and their relationship with properties of a corn crop. *Precision Agriculture*, *19*(6), 1127–1137. https://doi.org/10.1007/s11119-018-9570-9

Pandya, U., Mudaliar, A., & Gaikwad, A. (2023). Forecasting of banana crop productivity using geospatial approach: A case study of anand district. *ECWS-7 2023*. https://doi.org/10.3390/ecws-7-14248

Mohanasundaram, S., Kasiviswanathan, K. S., Purnanjali, C., Santikayasa, I. P., & Singh, S. (2022). Downscaling global gridded crop yield data products and crop water productivity

mapping using remote sensing derived variables in the South Asia. *International Journal of Plant Production*, *17*(1), 1–16. https://doi.org/10.1007/s42106-022-00223-2

Spiliotopoulos, M., Alpanakis, N., Tziatzios, G. A., Faraslis, I., Sidiropoulos, P., Sakellariou, S., Karoutsos, G., Dalezios, N. R., & Dercas, N. (2023a). Estimation of remotely sensed actual evapotranspiration in water-limited Mediterranean agroecosystems for monitoring crop (cotton) water requirements. *ECWS-7 2023*. https://doi.org/10.3390/ecws-7-14200

Darwish, M. A., Elkot, A. F., Elfanah, A. M., Selim, A. I., Yassin, M. M., Abomarzoka, E. A., El-Maghraby, M. A., Rebouh, N. Y., & Ali, A. M. (2023). Evaluation of wheat genotypes under water regimes using hyperspectral reflectance and agro-physiological parameters via genotype by yield*trait approaches in Sakha Station, Delta, Egypt. *Agriculture*, *13*(7), 1338. https://doi.org/10.3390/agriculture13071338

Li, H., Zheng, L., Lei, Y., Li, C., Liu, Z., & Zhang, S. (2008). Estimation of water consumption and crop water productivity of winter wheat in north China plain using Remote Sensing Technology. *Agricultural Water Management*, *95*(11), 1271–1278. https://doi.org/10.1016/j.agwat.2008.05.003

Dalla Marta, A., Eitzinger, J., Kersebaum, K.-C., Todorovic, M., & Altobelli, F. (2018). Assessment and monitoring of crop water use and productivity in response to climate change. *The Journal of Agricultural Science*, *156*(5), 575–576. https://doi.org/10.1017/s002185961800076x

Shoukat, M. R., Shafeeque, M., Sarwar, A., Mehmood, K., & Masud Cheema, M. J. (2021). Investigating effects of deficit irrigation levels and fertilizer rates on water use efficiency and productivity based on field observations and modeling approaches. *International Journal of Hydrology*, *5*(5), 252–263. https://doi.org/10.15406/ijh.2021.05.00287

Abou Zakhem, B., Al Ain, F., & Hafez, R. (2019). Assessment of field water budget components for increasing water productivity under drip irrigation in arid and semi-arid areas, Syria. *Irrigation and Drainage*, *68*(3), 452–463. https://doi.org/10.1002/ird.2286

Ruhoff, A. L., Paz, A. R., Collischonn, W., Aragao, L. E. O. C., Rocha, H. R., & Malhi, Y. S. (2012). A Modis-based energy balance to estimate evapotranspiration for clear-sky days in Brazilian tropical savannas. *Remote Sensing*, *4*(3), 703–725. https://doi.org/10.3390/rs4030703

Prakash Mohan, M. M., Rajitha, K., & Varma, M. R. (2019). Integration of soil moisture as an auxiliary parameter for the anchor pixel selection process in Sebal using Landsat 8 and Sentinel - 1A Images. *International Journal of Remote Sensing*, *41*(3), 1214–1231. https://doi.org/10.1080/01431161.2019.1658239

Bansouleh, B., Karimi, A., & Hesadi, H. (2015). Evaluation of sebal and SEBS algorithms in the estimation of maize evapotranspiration. *International Journal of Plant & Soil Science*, *6*(6), 350–358. https://doi.org/10.9734/ijpss/2015/15711

PACHAC HUERTA, Y. C., & CHÁVARRI VELARDE, E. A. (2019). Spatial estimation of maize evapotranspiration (Zea mays) using the SEBAL algorithm in the valley of Huaylas, Huaraz -Peru, in 2016. *38th IAHR World Congress - "Water: Connecting the World."* https://doi.org/10.3850/38wc092019-0321

Kamyab, A. D., Mokhtari, S., & Jafarinia, R. (2022). A comparative study in quantification of maize evapotranspiration for Iranian maize farm using Sebal and metric-1 EEFLUX algorithms. *Acta Geophysica*, *70*(1), 319–332. https://doi.org/10.1007/s11600-021-00704-4

Souza, P. J., Silva, E. R., Silva, B. B., Ferreira, T. R., Sousa, D. de, Luz, D. B., Adami, M., Sousa, A. M., Nunes, H. G., Fernandes, G. S., Pinto, J. V., Farias, V. D., Oliveira, I. A., Silva, S. A., Costa, J. F., Rua, M. L., Costa, D. L., Moura, V. B., Lima, M. J., … Ortega-Farias, S. (2023). Estimation of the evapotranspiration of irrigated açaí (Euterpe oleracea M.), through the surface energy balance algorithm for land—SEBAL, in Eastern Amazonia. *Water*, *15*(6), 1073. https://doi.org/10.3390/w15061073

Gibson, L., Jarmain, C., Su, Z., & Eckardt, F. (2013). Review: Estimating evapotranspiration using remote sensing and the Surface Energy Balance System – a South African perspective. *Water SA*, *39*(4). https://doi.org/10.4314/wsa.v39i4.5

Hassan, D., Abdalkadhum, A., Mohammed, R., & Shaban, A. (2022). Integration Remote Sensing and meteorological data to monitoring plant phenology and estimation crop coefficient and evapotranspiration. *Journal of Ecological Engineering*, *23*(4), 325–335. https://doi.org/10.12911/22998993/146267

Wang, Q.-Q., Geng, C.-X., Wang, L., Zheng, T.-T., Jiang, Q.-H., Yang, T., Liu, Y.-Q., & Wang, Z. (2023). Water conservation and ecological water requirement prediction of mining area in arid region based on RS-GIS and invest: A case study of bayan obo mine in Baotou, China. *Sustainability*, *15*(5), 4238. https://doi.org/10.3390/su15054238

Yihun, Y. M., Haile, A. M., Schultz, B., & Erkossa, T. (2013). Crop water productivity of irrigated teff in a water stressed region. *Water Resources Management*, *27*(8), 3115–3125. https://doi.org/10.1007/s11269-013-0336-x

Lim, C.-H., Kim, S., Choi, Y., Kafatos, M., & Lee, W.-K. (2017). Estimation of the virtual water content of main crops on the Korean peninsula using multiple regional climate models and evapotranspiration methods. *Sustainability*, *9*(7), 1172. https://doi.org/10.3390/su9071172

Talpur, Z., Zaidi, A. Z., Ahmed, S., Mengistu, T. D., Choi, S.-J., & Chung, I.-M. (2023). Estimation of crop water productivity using GIS and remote sensing techniques. *Sustainability*, *15*(14), 11154. https://doi.org/10.3390/su151411154

Ahmadpour, A., Farhadi Bansouleh, B., & Azari, A. (2022). Proposing a combined method for the estimation of spatial and temporal variation of crop water productivity under deficit irrigation scenarios based on the AQUACROP model. *Applied Water Science*, *12*(7). https://doi.org/10.1007/s13201-022-01666-8

Shan, Y., Li, G., Tan, S., Su, L., Sun, Y., Mu, W., & Wang, Q. (2023). Optimizing the maize irrigation strategy and yield prediction under future climate scenarios in the Yellow River Delta. *Agronomy*, *13*(4), 960. https://doi.org/10.3390/agronomy13040960

Mostafa, M., Luo, W., Zou, J., & Salem, A. (2023). Optimizing rice irrigation strategies to maximize water productivity: A simulation study using AQUACROP model for the Yanyun

Irrigation District, Yangzhou, China. *Earth*, *4*(3), 445–460. https://doi.org/10.3390/earth4030024

Sen, R., Zambreski, Z. T., & Sharda, V. (2023). Impact of spatial soil variability on rainfed maize yield in Kansas under a changing climate. *Agronomy*, *13*(3), 906. https://doi.org/10.3390/agronomy13030906

Cuculeanu, V., Tuinea, P., & Bălteanu, D. (2002). Climate change impacts in Romania: Vulnerability and adaptation options. *GeoJournal*, *57*(3), 203–209. https://doi.org/10.1023/b:gejo.0000003613.15101.d9

Kisekka, I., Schlegel, A., Ma, L., Gowda, P. H., & Prasad, P. V. V. (2017). Optimizing preplant irrigation for maize under limited water in the High Plains. *Agricultural Water Management*, *187*, 154–163. https://doi.org/10.1016/j.agwat.2017.03.023

Bekchanov, M., Lamers, J. P., Karimov, A., & Müller, M. (2011). Estimation of spatial and temporal variability of crop water productivity with incomplete data. *Cotton, Water, Salts and Soums*, 329–344. https://doi.org/10.1007/978-94-007-1963-7_20

International Committee of the Red Cross. (2022, December 5). *Kenya drought response: Facts & figures May - November 2022*. International Committee of the Red Cross. https://www.icrc.org/en/document/kenya-drought-response-facts-figures-may-november-2022

Muigai, D. K., Onwonga, R. N., Karuku, G. N., and Mohammed, A. Effect of irrigation schedules on maize (Zea mays l.) growth and yield in Bura irrigation scheme, Tana River County.

Mbayaki, C. W. (2021). Performance and water productivity of selected sweet potatoes (Ipomoea Batatas L) varieties intercropped with common beans in Katumani-Kenya. https://doi.org/http://dx.doi.org/10.13140/RG.2.2.25977.60000

Fan, M., Shen, J., Yuan, L., Jiang, R., Chen, X., Davies, W. J., & Zhang, F. (2011). Improving crop productivity and resource use efficiency to ensure food security and

environmental quality in China. *Journal of Experimental Botany*, *63*(1), 13–24. https://doi.org/10.1093/jxb/err248

Muli. N., M., R. N., O., G. N., K., V. M., K., & M. O., N. (2015). Simulating soil moisture under different tillage practices, cropping systems and organic fertilizers using CropSyst model, in Matuu Division, Kenya. *Journal of Agricultural Science*, *7*(2). https://doi.org/10.5539/jas.v7n2p26

Mulwa, F., Li, Z., & Fangninou, F. F. (2021). Water scarcity in Kenya: Current status, challenges and future solutions. *OALib*, *08*(01), 1–15. https://doi.org/10.4236/oalib.1107096

United Nations. (2022). *Goal 6 | Department of Economic and Social Affairs*. United Nations. https://sdgs.un.org/goals/goal6

Sadri, S., Famiglietti, J. S., Pan, M., Beck, H. E., Berg, A., & Wood, E. F. (2022). Farmcan: A physical, statistical, and machine learning model to forecast crop water deficit for farms. *Hydrology and Earth System Sciences*, *26*(20), 5373–5390. https://doi.org/10.5194/hess-26-5373-2022

Saini, R., & Ghosh, S. K. (2018). Crop classification on single date sentinel-2 imagery using random forest and support Vector Machine. *The International Archives of the Photogrammetry, Remote Sensing and Spatial Information Sciences*, *XLII–5*, 683–688. https://doi.org/10.5194/isprs-archives-xlii-5-683-2018

Vergopolan, N., Xiong, S., Estes, L., Wanders, N., Chaney, N. W., Wood, E. F., Konar, M., Caylor, K., Beck, H. E., Gatti, N., Evans, T., & Sheffield, J. (2021). Field-scale soil moisture bridges the spatial-scale gap between drought monitoring and agricultural yields. *Hydrology and Earth System Sciences*, *25*(4), 1827–1847. https://doi.org/10.5194/hess-25-1827-2021

Virnodkar, S. S., Pachghare, V. K., Patil, V. C., & Jha, S. K. (2020). Remote Sensing and machine learning for crop water stress determination in various crops: A critical review. *Precision Agriculture*, *21*(5), 1121–1155. https://doi.org/10.1007/s11119-020-09711-9

Patel, A., Singh, P. K., & Tandon, S. (2021). Weather prediction using machine learning. *SSRN Electronic Journal*. https://doi.org/10.2139/ssrn.3836085

Islam, M. D., Di, L., Qamer, F. M., Shrestha, S., Guo, L., Lin, L., Mayer, T. J., & Phalke, A. R. (2023). Rapid rice yield estimation using integrated remote sensing and meteorological data and machine learning. *Remote Sensing*, *15*(9), 2374. https://doi.org/10.3390/rs15092374

Elbeltagi, A., Srivastava, A., Kushwaha, N. L., Juhász, C., Tamás, J., & Nagy, A. (2022). Meteorological data fusion approach for modeling crop water productivity based on ensemble machine learning. *Water*, *15*(1), 30. https://doi.org/10.3390/w15010030

Gao, H., Zhang, X., Wang, X., & Zeng, Y. (2023a). Phenology-based remote sensing assessment of Crop Water Productivity. *Water*, *15*(2), 329. https://doi.org/10.3390/w15020329

Ghorbanpour, A. K., Kisekka, I., Afshar, A., Hessels, T., Taraghi, M., Hessari, B., Tourian, M. J., & Duan, Z. (2022). Crop water productivity mapping and benchmarking using remote sensing and Google Earth Engine Cloud Computing. *Remote Sensing*, *14*(19), 4934. https://doi.org/10.3390/rs14194934

Blatchford, M., Karimi, P., Bastiaanssen, W. G. M., & Nouri, H. (2018). From global goals to local gains—a framework for crop water productivity. *ISPRS International Journal of Geo-Information*, *7*(11), 414. https://doi.org/10.3390/ijgi7110414

Sarshad, A., Talei, D., Torabi, M., Rafiei, F., & Nejatkhah, P. (2021). Morphological and biochemical responses of sorghum bicolor (L.) moench under drought stress. *SN Applied Sciences*, *3*(1). https://doi.org/10.1007/s42452-020-03977-4

Hommadi, A. H., & Almasraf, S. A. (2019). Water retention techniques under crop's root zone a tool to enhance water use efficiency and economic water productivity for Zucchini. *Journal of Engineering*, *25*(6), 44–52. https://doi.org/10.31026/j.eng.2019.06.04

Booker, J. F., & Trees, W. S. (2020). Implications of water scarcity for water productivity and Farm Labor. *Water*, *12*(1), 308. https://doi.org/10.3390/w12010308

Hellegers, P. J., Soppe, R., Perry, C. J., & Bastiaanssen, W. G. (2008). Combining remote sensing and economic analysis to support decisions that affect water productivity. *Irrigation Science*, *27*(3), 243–251. https://doi.org/10.1007/s00271-008-0139-7

Appendix